Title
A Cryptochrome 2 mutation yields advanced sleep phase in humans

Journal
eLife, 5(AUGUST)

ISSN
2050-084X

Authors
Hirano, Arisa
Shi, Guangsen
Jones, Christopher R
et al.

Publication Date
2016

DOI
10.7554/elife.16695

Peer reviewed

A Cryptochrome 2 Mutation Yields Advanced Sleep Phase in Human

Arisa Hirano[1], Guangsen Shi[1], Christopher R. Jones[2], Anna Lipzen[3,4], Len A. Pennacchio[3,4], Ying-Xu[5], William C. Hallows[1], Thomas McMahon[1], Maya Yamazaki[1], Louis J. Ptáček[1,6*], Ying-Hui Fu[1*]

[1]Department of Neurology, University of California San Francisco, San Francisco, 94143, CA

[2]Department of Neurology, University of Utah, Salt Lake City, UT

[3]Lawrence Berkeley National Laboratory, Berkeley, CA

[4]Department of Energy Joint Genome Institute, Walnut Creek, CA

[5]Center for System Biology, Soochow University, Suzhou, China

[6]Howard Hughes Medical Institute, University of California San Francisco, San Francisco, CA

*Correspondence:L.J.P. (ljp@ucsf.edu), Y-H.F. (Ying-Hui.Fu@ucsf.edu).

Abstract

Familial Advanced Sleep Phase (FASP) is a heritable human sleep phenotype characterized by very early sleep and wake times. We identified a missense mutation in the human Cryptochrome 2 (*CRY2*) gene that co-segregates with FASP in one family. The mutation leads to replacement of an alanine residue at position 260 with a threonine (A260T). In mice, the *CRY2* mutation causes a shortened circadian period and reduced phase-shift to early-night light pulse associated with phase-advanced behavioral rhythms in the light-dark cycle. The A260T mutation is located in the phosphate loop of the flavin adenine dinucleotide (FAD) binding domain of CRY2. The mutation alters the conformation of CRY2, increasing its accessibility and affinity for FBXL3 (an E3 ubiquitin ligase), thus promoting its degradation. These results demonstrate that CRY2 stability controlled by FBXL3 plays a key role in the regulation of human sleep wake behavior.

Introduction

Sleep is vital for all animals. Sleep-wake timing is regulated by the internal biological clock driving physiological rhythms with a period of approximately 24 hours (Takahashi, 1995). The circadian clock is composed of interlocked transcriptional and translational negative feedback loops (Lowrey and Takahashi, 2004; Reppert and Weaver, 2001). In mammals, a CLOCK-BMAL1 heterodimer binds to E-boxes and activates gene expression of the *Period* (*Per*) and *Cryptochrome* (*Cry*) genes. Translated PERs and CRYs proteins form a complex that enters the nucleus to inhibit their own transcription through direct interaction with CLOCK-BMAL1 heterodimers. PER and CRY proteins accumulating in the nucleus are then degraded over time. As protein levels fall (depending on rate of degradation), the transcription-translation feedback loop begins anew.

CRY2 is a principal component in mammalian circadian clocks (Shearman et al., 2000; van der Horst et al., 1999; Vitaterna et al., 1999). While Drosophila and plant CRY proteins act as photoreceptors contributing to photoentrainment of the circadian clock and other biological processes by binding to flavin adenine dinucleotide (FAD) (Partch and Sancar, 2005), mammalian CRY2 has light-independent transcriptional repressor activity and strongly inhibits E-box-regulated gene expression (Griffin et al., 1999; Kume et al., 1999; Shearman et al., 2000). The protein stability of CRY2 is fine-tuned by post-translational modification including phosphorylation and ubiquitylation. In addition, various enzyme modifications play a role in CRY2 regulation (Reischl

and Kramer, 2011; Stojkovic et al., 2014). Among them, FBXL3 is an F-box type E3 ubiquitin ligase which promotes CRY1 and CRY2 ubiquitylation thus leading to proteasome-mediated degradation (Busino et al., 2007). Mutations in mouse *Fbxl3* or knockout of the *Fbxl3* gene dramatically lengthens the period of mouse behavioral rhythms in constant darkness (Godinho et al., 2007; Hirano et al., 2013; Shi et al., 2013; Siepka et al., 2007), indicating that the protein stability of CRY1 and CRY2 is a critical determinant of circadian period in mice. However, direct evidence supporting the significance of *CRY2* and the post-translational regulation of CRY2 protein in the human circadian clock regulating the sleep-wake cycle has been lacking.

Familial Advanced Sleep Phase (FASP) is a heritable sleep phenotype characterized by stable early sleep and wake times (Jones et al., 1999; Reid and Burgess, 2005; Reid et al., 2001). The FASP phenotype can segregate as a highly penetrant, autosomal dominant trait in human kindreds. Previously, we have identified mutations in clock genes, including *Period2, Period3*, *casein kinase I*δ, and *Dec2* causing circadian and sleep homeostasis phenotypes in humans (He et al., 2009; Toh et al., 2001; Xu et al., 2005; Zhang et al., 2016). A mutation at the phosphorylation priming site of PER2 attenuates sequential phosphorylation and consequently destabilizes PER2 proteins. The mouse model expressing mutant PER2 exhibits a shortened circadian period accompanied with large phase-advance in sleep-wake rhythms (Xu et al., 2007). This sequential phosphorylation region of PER2 was later found to be modulated

by another post-translational regulation, *O*-GlcNAcylation, demonstrating an interplay and competition between phosphorylation and *O*-GlcNAcylation of serine residues in this region (Kaasik et al., 2013). These studies highlighted the important role of post-translational regulation of clock proteins *in vivo* in humans and also revealed mechanistic insight into the regulation of PER2. Thus, human genetic studies have provided valuable and unique opportunities to elucidate novel molecular mechanisms of circadian/sleep regulation.

Here we report the identification of a novel variant in the human h*CRY2* gene that leads to FASP. Generation of a mouse model carrying the mutation revealed that the mutation causes a FASP-like phenotype in mice with altered circadian period and photic entrainment. We found that the mutation in the CRY2 FAD-binding-domain enhances its affinity for FBXL3, thus destabilizing CRY2 via increased ubiquitylation and targeting for degradation by the proteasome. We conclude that regulation of CRY2 stability by a proper balance of FAD and FBXL3 is essential for the sleep-wake cycle in humans.

Results

Identification of a novel mutation in the h*CRY2* gene associated with FASP

Through candidate gene screening in FASP families, we identified a missense mutation in the human *CRY2* gene, which causes an amino acid conversion from Ala→Thr at position 260 (A260T) (Figure 1A). No other novel mutations were found in ~25 candidate circadian genes that were sequenced. The A260T

mutation is associated with the circadian phenotype in this FASP family (Figure 1A) (Jones et al., 1999; Toh et al., 2001; Xu et al., 2005; Zhang et al., 2016). The fraternal twin sisters inherited the mutation from their mother and both reported a strong morning preference (Horne-Ostberg scores of 84 and 72) (Figure 1-source data 1). The proband also had a very early melatonin onset (4:41 P.M.), while the averaged melatonin onset of normative samples is 8:50 P.M. (Burgess and Fogg, 2008). Her melatonin onset time is 3.35 standard deviations earlier than expected and among the earliest 0.05% of normative samples (Burgess and Fogg, 2008). Ala260 is located in the FAD binding domain of CRY2 and it is highly conserved in CRY1 and CRY2 proteins of various species (Figure 1B).

FASP in mouse model carrying A260T mutation

To test whether the A260T mutation causes FASP and has a dominant effect on the circadian sleep-wake cycle, we generated wild-type h*CRY2* (h*CRY2-WT*) and mutant h*CRY2* (h*CRY2-A260T*) human BAC transgenic (Tg) mice (Figure 2-supplement 1A). Transgenic mice were subjected to locomotor behavioral analysis using a video camera tracking system. Under conditions of 12-hr light and 12-hr dark (LD 12:12), both h*CRY2-WT* and h*CRY2-A260T* mice entrained stably to the LD cycle (Figure 2A). However, the peak time of resting behavior, as determined by quadratic-function fitting, was significantly advanced in h*CRY2-A260T* mutant mice (Figure 2B). The activity offset and onset times were also advanced in h*CRY2-A260T* mutant mice vs. h*CRY2-WT* mice (Figure 2C

and Figure 2-supplement 1B). Similarly, h*CRY2-A260T* mutant mice on a *Cry2* null background demonstrated advanced activity onset and offset, especially around the LD transition (ZT12-13) (Figure 2-supplement 1C). These results demonstrate that h*CRY2-A260T* mice recapitulate the advanced sleep phase seen in the human FASP subjects harboring the *CRY2* mutation.

Shortened period and reduced phase-shift in h*CRY2-A260T* **mice**

We next analyzed voluntary wheel-running activity to evaluate phase-shift and free-running period of the circadian clock for the Tg mouse models. Similar to locomotor activity measured by video tracking (Figure 2A), wheel-running activity offset times were advanced in h*CRY2-A260T* vs. h*CRY2-WT* in LD on both m*Cry2* WT and null backgrounds (Figure 2D; Figure2-supplements 2), while there are no significant differences in activity onset time and acrophase. Interestingly, h*CRY2-A260T* showed reduced phase-delay when mice were subjected to a 30-min light pulse at ZT14 (Figure 2D, E), whereas phase-advance was normal in response to a light pulse at ZT22 (Figure 2-supplement 3). Thus, mutant mice have reduced sensitivity to entrainment by light at early night compared to control mice. The mice were subsequently released into constant darkness (DD) to determine circadian period. The free-running period of h*CRY2-A260T* (23.52+/-0.04 hr) was significantly shorter than that of h*CRY2-WT* (23.70+/-0.03 hr) and *WT* mice (23.74+/-0.02 hr) (Figure 2F). The period shortening phenotype was further enhanced by crossing Tg

mice onto the m*Cry2* null background (Figure 2-supplement 4A). The shorter circadian period and reduced phase-delay were also observed in another mutant line (23.51+/-0.06 hr) with a higher mutant transgene copy number (Figure 2-supplement 1A, 4B), thus excluding the possibility that the phenotype was due to positional effects of the transgene insertion site in the genome. Of note, there is no significant difference in the periods and phase-shifting of h*CRY2-WT* transgenic vs. transgene negative mice (Figure 2E, F), indicating that the shortening of circadian period and abnormal phase-delay are not simply due to overexpression of h*CRY2*. Taken together, these data demonstrate that the phase-advances in mice and humans results from the *CRY2* mutation. Data from the transgenic mice suggests that the phase advance may be due to a combination of shortened period *and* altered sensitivity to photic entrainment.

Shortened circadian period in peripheral clocks of h*CRY2-A260T*

The effect of the mutation on the circadian period and phase angle in the peripheral clock was examined by crossing BAC transgenic mice with m*Per2*^{LUC} knock-in mice (Yoo et al., 2004). Consistent with the behavioral rhythms, shortened clock period was observed in PER2::LUC bioluminescence rhythms of liver and lung cultures from h*CRY2-A260T* vs. WT mice (Figure 3A, B). The peak and trough time of the bioluminescence rhythms were advanced in both tissues of h*CRY2-A260T* mice, suggesting that phase of the peripheral clock is also advanced by the mutation *in vivo* (Figure 3C). Circadian period shortening

by the A260T mutation was also found using mouse embryonic fibroblasts (MEFs) derived from mice with a mutant vs. WT transgene on both WT and m*Cry2* knockout backgrounds (Figure 3D, E). In addition, NIH3T3 cells stably expressing CRY2-A260T also displayed a shorter circadian period than CRY2-WT expressing cells (Figure 3F), emphasizing the dominant effect of CRY2-A260T on the circadian period. Our results indicate that CRY2-A260T shortens the circadian period in both central and peripheral clocks, consistent with current understanding that core clock genes such as *Cry2* influence physiologies in multiple mammalian organ systems.

Destabilization of CRY2 protein by the A260T mutation

The CRY2 Ala260 residue resides in the “phosphate loop” responsible for binding to the phosphate of FAD (Hitomi et al., 2009) (Figure 1B). Mutations at amino acid residues critical for FAD binding affect CRY2 repressor activity of E-box-mediated transcriptional activation (Czarna et al., 2013; Hitomi et al., 2009; Sanada et al., 2004). Furthermore, Ser265 of mouse CRY2 (homologous residue of Ser266 in human CRY2) is a phosphorylation site, and the S265D mutation, mimicking a phosphorylated serine 265, reduces CRY2 repressor activity (Sanada et al., 2004). Using a Luciferase assay, we found that the A260T mutation weakened CRY2 repressor activity on *Per1* E-box-mediated transcriptional activation by CLOCK-BMAL1 (Figure 4A). However, the nuclear CRY2 protein levels in culture cells were decreased by the mutation (Figure 4B),

which could potentially account for the reduction of CRY2 repressor activity (Figure 4A). We then examined the degradation of CRY2 proteins by cycloheximide (CHX) chase experiments. Consistent with the cellular distribution of CRY2 (Figure 4B), CRY2-A260T was less stable than CRY2-WT in HEK293 cells, especially in the nucleus (Figure 4C). Destabilization of CRY2 by the mutation was further verified in a CRY2-LUC based bioluminescence degradation assay, where the protein decay rate can be determined by recording CRY2-LUC bioluminescence in culture (Hirano et al., 2013; Hirota et al., 2012) (Figure 4-supplement 1A). Although Ala260 does not directly bind to FAD (Hitomi et al., 2009), amino acid conversion from the hydrophobic and small amino acid, alanine, to threonine could alter the conformation of the phosphate loop. This idea is supported by an observation that a mutation from alanine to aspartic acid (A260D) caused a more severe effect on CRY2 repressor activity and protein stability than the A260T mutation (Figure 4-supplement 1A, B). We found that human CRY1 harboring the corresponding mutation at position 241 is less stable than CRY1-WT, suggesting a common regulatory mechanism for CRY1 and CRY2 by FAD binding (Figure 4-supplement 1C). These results indicate that the conformation of the phosphate loop may play critical roles in regulating CRY2 stability and repressor activity.

A260T mutation affects FBXL3-CRY2 interaction

FBXL3 primarily localizes in the nucleus and promotes proteasomal degradation

of CRY2, consequently having a strong impact on the circadian period of mice (Busino et al., 2007; Godinho et al., 2007; Siepka et al., 2007; Stojkovic et al., 2014). A previous structural study demonstrated that C-terminal region of FBXL3 interacts with CRY2 through the FAD binding pocket and mutations in the FAD binding domain alter CRY2-FBXL3 interaction (Xing et al., 2013). We therefore speculated that the A260T mutation affects the FBXL3-CRY2 interaction, thus altering CRY2 protein stability. We first examined WT and mutant CRY2 stability in the absence of FBXL3. As anticipated, h*FBXL3* knockdown in HEK293 cells increased the stability of both CRY2-WT and CRY2-A260T. Interestingly, the destabilizing effect of the A260T mutation was abrogated by h*FBXL3* knockdown (Figure 5A), suggesting the effect of the mutation requires FBXL3.

FAD stabilizes CRY2 by structurally interfering with the interaction between FBXL3 and CRY2 (Xing et al., 2013). We found that treatment of HEK293 cells with FAD increased CRY2-WT protein levels much more than CRY2-A260T (Figure 5B), suggesting that stabilization of CRY2 by FAD was reduced by the mutation. This result supports the hypothesis that the A260T mutation alters the FBXL3-CRY2 interaction. We thus carried out a competitive assay by adding FAD to complexed CRY2-FBXL3 to examine the effect of the mutation on the release of CRY2 from purified CRY2-FBXL3 complexes *in vitro*. Free CRY2-WT protein levels increased with addition of FAD in a dose-dependent manner (Figure 5C). In contrast, mutant CRY2 was released less readily than CRY2-WT from the complexes even though both forms of

CRY2 were bound to FBXL3 at the same level (Figure 5C). In addition, we tested FBXL3-mediated CRY2 degradation using KL001, a small synthetic molecule known to stabilize CRY1 and CRY2 (Hirota et al., 2012) due to its structural similarity to FAD (Nangle et al., 2013). KL001 stabilizes CRY2-WT in a dose-dependent manner as was previously reported (Hirota et al., 2012). However, KL001 failed to stabilize CRY2-A260T to the same extent it did for CRY2-WT (Figure 5D, Figure 5-supplement 1A). These results indicate that the A260T mutation weakened the function of FAD and KL001 as inhibitors of FBXL3-mediated degradation of CRY2 and that CRY2-A260T is less stable than CRY-WT, likely due to strengthened interaction with FBXL3. To determine whether the A260T mutation indeed modifies the interaction of CRY2 and FBXL3, we performed co-immunoprecipitation analysis. As expected, CRY2-A260T binds more strongly to FBXL3 than CRY2-WT in HEK293 cells (Figure 5E), consequently leading to more ubiquitylation of the mutant protein (Figure 5F). The effect of the mutation on the binding affinity under *in vivo* conditions will need to be further evaluated when better human CRY2 antibodies (for immunoprecipitation) become available.

We next performed structural modeling of mutant CRY2 to address how the A260T mutation modulates conformation of the phosphate loop. For modeling, we used the mouse CRY2 structure as the crystal structure of mouse CRY2-FBXL3 complex is available (Xing et al., 2013) and amino acid sequence in the phosphate loop perfectly conserved (Figure 1B). The published

CRY2-FBXL3 structure (Xing et al., 2013) revealed that space between Ala260 (corresponding to A259T in mouse) and Asp442 (mouse Asp441) in FBXL3-binding form (red) is more opened vs. the FAD-binding form (orange, Figure5-supplement 1B). The amino acid change from Ala260 to Thr increases molecular density in this space and may alter electrostatic interactions between Ala260Thr and Asp442. As a result, the mutation likely renders the CRY2-A260T more accessible to FBXL3 binding (Figure5-supplement 1C). This model is consistent with the results from CRY2-A260D mutation (Figure4-supplement 1). Taken together, we demonstrated that the A260T mutation in the FAD binding pocket endows mutant CRY2 with a higher accessibility and affinity for FBXL3, therefore leading to faster proteasomal degradation of mutant vs. wild-type CRY2.

Decreased endogenous CRY2 protein levels in h*CRY2-A260T* mice

Our *in vitro* studies demonstrate that CRY2-A260T is less stable than CRY2-WT (Figure 4). To examine the protein levels of mutant vs. wild-type CRY2 under physiological conditions, we used MEFs prepared from transgenic mice. Total protein levels of endogenous CRY2 were significantly lower in synchronized cells derived from h*CRY2-A260T* vs. h*CRY2-WT* mice at two different time points (Figure 6A), even though *Cry2* transcript levels in h*CRY2-A260T* mice was higher than in h*CRY2-WT* mice (Figure 6B). Similarly, CRY2 protein levels from liver nuclear extracts were lower in h*CRY2-A260T* vs. h*CRY2-WT* mice

288 (Figure 6C, D), while h*CRY2* mRNA levels were higher in mutant mice (Figure
289 6E). CRY1 protein levels were also decreased by the mutation in nuclear
290 extracts from liver (Figure 6C, D), suggesting that CRY1 is destabilized in
291 h*CRY2-A260T* mice. At the same time, we found that nuclear expression of
292 PER1 and PER2 were up-regulated in liver extracts from mutant mice,
293 particularly at ZT14 (Figure 6C, D), suggesting that the timing of nuclear
294 accumulation of PER proteins is advanced in h*CRY2-A260T* mice. Although
295 PER1 and PER2 protein levels were significantly altered, their mRNA levels
296 were not different (Figure 6E). A similar alteration of PER1 and PER2 protein
297 levels in the absence of noticeable changes in mRNA levels was previously
298 reported for *Psttm* mutant mouse liver (Yoo et al., 2013). *Psttm* mice have a
299 mutation in the *Fbxl21* gene and this mutation decreases the protein level of
300 FBXL21, which functionally competes with FBXL3. The *Psttm* mutation resulted
301 in CRY1 and CRY2 protein destabilization and a shorter circadian period in mice
302 (Yoo et al., 2013), which parallels the phenotype of our h*CRY2-A260T* mice
303 (Figure 2E). We found that the expression of clock genes in liver was not
304 significantly altered by the mutation, while the effect was obvious in MEFs
305 (Figure 6B, E, and Figure 6-supplement 1). This is congruent with a previous
306 suggestion that the effect of the CRY2 destabilization has diverged among
307 different tissues (Hirano et al., 2013; Yoo et al., 2013). Collectively, we
308 demonstrated that the A260T mutation destabilizes CRY2 proteins *in vivo,* likely
309 through alteration of FBXL3-mediated CRY2 degradation, leading to

perturbation of the circadian clock.

Discussion

We report here a mutation in h*CRY2* that causes FASP in humans. We initially identified this as a novel variant. Since that time, it has been recognized as a rare variant in the SNP database (rs201220841). The frequency of the A260T allele (0.00008 in the ExAc database) is much lower than that of FASP (0.5%, our unpublished data) in the general population. This is consistent with the A260T variant found in one of our FASP families being responsible for a small portion of FASP in the general population.

Among the mutation carriers of this family (Figure 1A), the proband, her twin sister, and her mother have clear advanced sleep phase. In contrast, the nephew of the proband (101374) did not have early sleep onset and offset although his genotype is A/G (Figure1-source data). Considering his age, we classified him as “unknown”, since adolescents and young adults are typically more difficult to categorize as having a definite circadian phenotype due to normal phase delays seen in many people beginning in adolescence and persisting into young adult life (boys/men > than girls/women) (Roenneberg et al., 2004). When phenotyped at age 21, subject 101374 was at the statistical peak age of maximum phase delay due to these developmental effects and was prone to be even more phase-delayed by his male sex. Therefore, he may become progressively more phase advanced as he grows older as a result of the *CRY2*

FASP allele as it is unmasked by these developmental changes. It is also possible that the mutation may not have 100% penetrance and therefore the nephew will never manifest the FASP trait.

In order to confirm that the A260T mutation is causative of FASP, we generated mice carrying the mutation and subjected them to detailed behavioral analysis (Figure 2). Consistent with the other FASP mutations previously reported (in h*CK1*δ and h*PER3,* the effects of the human mutation observed in mouse models and *in vitro* are subtle compared to those found in forward mutagenesis screens. This is expected since the mutations that we identified are found in extant humans in the “real world”. The circadian body clock plays crucial roles in maintaining normal physiological functions. Thus, any mutation manifesting the strong phenotypes seen in mutagenesis screens would almost certainly have been a selective disadvantage if they arose spontaneously in humans. Furthermore, while the phase advance in mice carrying the human *PER2* mutation appears to be due largely to a shortening of circadian period, the published *PER3* mice and the *CRY2* mice reported here both have altered entrainment. We speculate that some of FASP in humans is caused by altered entrainment properties that would not have been detected in forward mutagenesis screens because they have focused almost entirely on measuring period (not phase) as the target phenotype.

Previously, we have used wheel-running behavior analysis to characterize mouse models carrying human FASP mutations (Xu et al., 2007;

354 2005). Here, we investigated an additional behavior analysis method. For the
355 h*CRY2-A260T* mouse model, we also employed continuous video recording
356 (Figure 2A and Figure 2-supplement 1). We found that video recording was quite
357 sensitive to detect advanced sleep phase (Figure 2A-C and Figure
358 2-supplement 1). Although wheel-running also displays the phase advance of
359 activity offset in the h*CRY2-A260T* mice (Figure 2-supplement 2), the data from
360 wheel-running is less robust for detecting a phase advance of activity onset. This
361 is likely due to a strong light-masking effect for mouse at the light-to-dark
362 transition for activity onset. Thus, when the lights are on, mice are less likely to
363 run on a wheel. However, smaller amplitude movements like grooming behavior
364 and moving in the cage were detected by video recording. Wheel running was
365 quite sensitive to detect phase advance of activity offset as this is seen during
366 the dark phase of LD 12:12.

367 In this study, we found that the circadian period was significantly
368 shortened by the A260T mutation in the central and peripheral clocks (Figure 2F,
369 3A-E). Growing evidence indicates that stability of CRY proteins dominantly
370 determines the circadian period length (Godinho et al., 2007; Hirano et al., 2014;
371 Shi et al., 2013; Siepka et al., 2007; St John et al., 2014): stabilization of CRY
372 lengthens circadian period in mice whereas destabilization of CRY shortens the
373 period. Consistent with this model, our human mutation destabilizes CRY2 and
374 leads to a short circadian period of mouse behavioral rhythms (Figure 6F).
375 Shortened circadian periods have been measured in one FASP human subject

(Jones et al., 1999), and in mouse models of human FASP mutations (Xu et al., 2007; 2005). Mutant animals having a shorter free-running period such as *tau* mutant hamster also tend to exhibit advanced phase of behavioral rhythms in LD (Lowrey et al., 2000). Thus, it is likely that the *CRY2* mutation results in FASP, at least in part, through shortening of the free-running period.

Interestingly, our data also indicates that another circadian clock feature, phase resetting by light, is dysregulated in the h*CRY2* mutant mouse model. h*CRY2-A260T* mice have a smaller phase-shift in response to a light pulse in early subjective night compared to h*CRY2-WT* mice (Figure 2E; Figure 2-supplement 3). In order to live on a 24 hour day in LD 12:12, wild-type mice need to phase delay a small amount each day because the endogenous circadian period is slightly shorter than 24 hours. A reduced ability to phase-delay observed in the h*CRY2-A260T* mouse model could contribute to advanced sleep phase, though the mechanism for the altered phase-shift remains to be elucidated. Although the difference in the free-running period of the transgenic mice was subtle as compared to the degree of phase-advance manifested in human mutation carriers or mice carrying the mutant h*PER2* transgene (Figure 2B, F), it is reasonable to expect that the alteration of both circadian period and light-induced phase-shifting together will strongly influence the phase angle of entrainment. The *after-hours* mutation in the mouse *Fbxl3* gene causes stabilization of CRY leading to an extremely long circadian period (Godinho et al., 2007). These mutant mice also exhibit large phase-shifts in

response to light (Guilding et al., 2013). The authors speculated that reduced amplitude of the circadian clock in *after-hours* mutant mice leads to the abnormal enhancement of phase-resetting. In this study, the A260T mutation elevated PER1 and PER2 levels, especially at ZT14, and the amplitude of PER1 protein rhythm was greater in h*CRY2-A260T* vs. h*CRY2-WT* mice (Figure 6D). Thus, the effect of light pulses in the early night may be decreased by the perturbed protein profiles (increased amplitude) of PER1 and PER2 in h*CRY2-A260T* mice.

FAD is a chromophore binding to flavo proteins regulating various biological processes and it is required for the light-sensing activity of CRY in various species (Lin and Todo, 2005; Partch and Sancar, 2005). *Drosophila* CRY is degraded by the proteasome in response to light signals, which is a trigger for phase-resetting of the circadian clock in flies. However, the ability of mammalian CRYs as a photoreceptor remains controversial as double knockout mice of *Cry1* and *Cry2* are still able to entrain to light and show *Per1* gene induction in SCN in response to light pulses (Okamura et al., 1999). These double knockout mice completely lack behavioral rhythms in constant darkness (van der Horst et al., 1999). Furthermore, the repressor activity of CRY on E-boxes and its interaction with other clock proteins are independent of light (Griffin et al., 1999). These findings emphasize the light-independent role of CRY proteins in mammals. Thus, the physiological role of FAD binding in the mammalian clock has been totally unknown, while a previous study implied that

FAD can structurally compete with FBXL3. Our findings provide the first evidence that FAD functions as a stabilizer of CRY2 protein by modulating FBXL3-CRY2 interaction (Figure 5). The results presented here demonstrate that the protein stability of CRY2 regulated by the balance of FBXL3 and FAD controls clock speed and sleep/wake timing in mice and humans.

Several genetic studies reported that the human *CRY2* gene is associated with mood regulation, cancer and glucose homeostasis (Dupuis et al., 2010; Hoffman et al., 2010; Kovanen et al., 2013; Lavebratt et al., 2010; Sjöholm et al., 2010; Zhang et al., 2013). Although psychiatric disorders, cancer, and metabolic disorders are tightly connected with dysfunction of the biological clock, associations of CRY2 polymorphisms with morning/evening preference or other circadian phenotypes have not been described. One polymorphism in the *FBXL3* gene was reported to be associated with diurnal preference (Parsons et al., 2014), implying the conserved role of FBXL3 in the human circadian clock. However, it remains to be elucidated whether that variant in *FBXL3* is causative (vs. merely be associated with) the human circadian phenotype and whether it acts through CRY regulation. Here, we demonstrate that regulatory mechanisms for CRY2 protein are well conserved between mice and humans and that control of CRY2 stability is critical for appropriate phase angle and period of the circadian clock in humans.

Material and Methods

Method Summary

All human subjects signed a consent form approved by the Institutional Review Boards at the University of Utah and the University of California, San Francisco (IRB# 10-03952). The consent form includes all confidentiality and ethic guidelines and also indicates not revealing subject information in the publication. All experimental protocols (Protocol no. AN111686-02) were conducted according to US National Institutes of Health guidelines for animal research and were approved by the Institutional Animal Care and Use Committee at the University of California, San Francisco.

Human data and mutation screening

Subjects were characterized by a previously published procedure established by one of the authors (CRJ, Jones et al., 1999). The data were interpreted by one of the authors (CRJ) as possible, probable, definite, or severe advanced sleep phase syndrome by at least age 30. Though ancillary features of ASP (earlier spontaneous wake time if an earlier bed time is selected) and potential confounding or masking influences were considered, most participants categorized as “definite ASP” reported spontaneous vacation sleep onset and offset time no later than 21:30 and 05:30, respectively and had H-O score (or numerically equivalent childhood MEQ score) of at least 72. We considered children and adolescents more difficult to categorize as having a definite,

life-long circadian phenotype unless it was severe by all measures including DLMO phase. DNAs purified from blood samples were used to screen for mutations.

The salivary dim light melatonin onset (DLMO) of the proband was obtained on the last night of the home recordings. DLMO phase was assessed from serial saliva samples (~1 mL) collected at 30 minutes intervals using “Salivette” saliva collection tubes (Sarstedt, Inc., Newton, NC) in dim light (</=10 lux) confirmed by recording the ambient light level before each sample using a luxmeter (Sinometer, ShenZhen, China). Samples were collected, beginning 6 hours before the subject’s typical bedtime. Saliva samples were frozen overnight and then shipped the next day in an insulated box with frozen coolant to another laboratory (Solid Phase, Portland, Maine) for radioimmunoassay by test kit (APLOCO Diagnostics, Windham, NH). The lower limit of detection of this assay is 0.2 pg/mL. The salivary dim light melatonin onset (DLMO) in adults was calculated and compared with a population sample not purposely selected for morning or evening preference by the method and data of Burgess and Fogg (Burgess and Fogg, 2008). Concurrent sleep logs and Zeo (Zeo Incorporated, Newton, Massachusetts) EEG recordings were obtained for ten consecutive nights of sleep at home. DNAs purified from blood samples were used to screen for mutations. For this particular family, a list of candidate genes including *CLOCK, BMAL1, PER1-3, CRY1-2, DEC1-2, CSNK1D, CSNK1E, PRKAA2, NPAS2, CSNK2A2, CSNK2B, FBXL3, GSK3B, PKCA, PRKAA1, PRKAA2,*

RAB3A, RORA, TIMELESS, NR1D1, and PRKCG were screened. CRY2 (Accession number; EAW68030) A260T was identified as a novel variant specific for mutation carriers of this family (at the time of identification in 2008). The prevalence of the A260T allele (rs201220841) is 0.008% and 0.1% in the two sets of public genome databases, of which sample sizes are 121,412 and 1,323, respectively.

Engineering of BAC constructs for generating transgenic mice

A human BAC RP11-1084E2 containing the entire CRY2 gene on a 189 kb genomic insert was obtained from CHORI (Children's Hospital Oakland Research Institute). The BAC clone was modified by homologous recombination using the Counter-Selection BAC Modification Kit (Gene Bridges GmbH) as previously described (Lee et al., 2012). Briefly, a linear PCR fragment containing a streptomycin/kanamycin counter selection gene was amplified. The primers for this reaction were designed so that 20 nucleotides would anneal to the streptomycin/kanamycin gene and an additional 40 nucleotides homologous to sequences flanking the mutation site. This PCR product was transferred into the RP11-1084E2 BAC to initiate homologous recombination in the DH10B *Escherichia coli* strain that already contained the plasmid pSC101- BAD-gbaA^{tet}**.** The counter selection gene was then removed by a second recombination event using an oligonucleotide carrying the mutation (G-to-A) in the center. All relevant segments generated by PCR and recombination were sequence confirmed.

Detailed mapping was carried out for the modified BACs to ensure that correct constructs were obtained. Transgenic mice were generated using standard microinjection procedures. The transgenic founders were on a C57BL/6 × SJL F_1 background and were backcrossed to C57BL/6 mice in successive generations. The copy number for each transgenic line was calculated by quantitative real-time PCR using common sequences for mouse *Cry2* (reference) and human *CRY2* genes.

Purchased mouse lines

m*Per2*^{Luc} knockin mice (RRID IMSR_006852) and m*Cry2* knockout mouse (RRID IMSR_016185) were purchased from The Jackson Laboratory and crossed with h*CRY2* transgenic mice.

Wheel-running analysis of transgenic mice

All mice tested were ~8 week-old males maintained on a C57BL/6J background. Mice were kept in individual wheel running cages with free access to food and water. First, mice were entrained to LD 12:12. Activity profiles, offset time and acrophase were analyzed using data from day 10 to day 14 in LD. After entrainment to LD for approximately 3 weeks, mice were released into constant darkness (DD) for measurement of free-running period. Circadian periods were calculated by line fitting of activity onsets from day 7 to day 19 in DD. To analyze for phase-shifts, mice were given a 30 min-light pulse (200 lux) beginning at

ZT14 (2 hours after lights-off) or at ZT22 (2 hours before lights-on), and then released into DD. Phase-shifts were determined by line fitting of activity onsets from day1 to day7 in DD. All data collection and analysis was done using ClockLab software (Actimetrics, Wilmette, IL; RRID SCR_014309). Activity onset and offset were defined using the ClockLab software algorithm. The default template is 6 hours of inactivity followed by 6 hours activity for onset (or vice versa for offset).

ANY-maze analysis of transgenic mice

All mice tested were ~16 week-old males maintained on a C57BL/6J background. Mice were kept in individual cages with free access to food and water. Mice were monitored by infrared camera and tracked by an automatic video tracking system (Storlting, Wood Dale, IL; RRID SCR_014289). Mice were entrained to LD 12:12 for 1 week and then locomotor activity was recorded for 3 or 4 days. Walking distance and immobility times were calculated using ANY-maze software and data were averaged. Samples with over 500-meter walking distance or below 10,000-sec immobility time each day were excluded from the statistical analysis due to the failure of automatic tracking.

Cell culture and constructs

HEK293 cells (ATCC CRL-1573; RRID CVCL_0045) and NIH 3T3 cells (ATCC CRL-1658; RRID CVCL_0594) were purchased from ATTC. Authentication of

the cell lines was performed using STR profiling by ATCC. Mycoplasma contamination was checked every 6 months and mycoplasma-free cell lines were used for all experiments in this study. Cells were cultured in DMEM (Sigma Aldrich) containing 10% FBS and 100 U/ml Penicillin-Streptomycin (Life Technologies) and maintained by standard methods. Mouse embryonic fibroblasts (MEFs) were prepared from E12.5 embryos of h*CRY2-WT* and h*CRY2-A260T* transgenic mice. After removing the head, paws and internal organs, embryos were chopped and incubated in 0.25% trypsin in PBS for 24 hr at 4°C. After incubation for 20 min at 37°C in 0.25% trypsin in PBS, cells were dissociated by pipetting in DMEM. Supernatant was cultured in a cell culture dish with DMEM and maintained by standard methods. Cells were transfected with Lipofectamine 3000 transfection reagent (Life Technologies) according to manufacturer's protocol. DNA constructs used for transfections are as follows: hCRY2-WT-Myc-His/pcDNA3.1, hCRY2-A260T-Myc-His/pcDNA3.1, hCRY2-A260D-Myc-His/pcDNA3.1, hCRY2-WT-HA/pCMV-tag2B, hCRY2-A260T-HA/pCMV-tag2B, FLAG-hCRY2-WT/p3×FLAG-CMV-10, FLAG-hCRY2-A260T/p3×FLAG-CMV-10, FLAG-hCRY1-WT/p3×FLAG-CMV-10, FLAG-hCRY1-A241T/p3×FLAG-CMV-10, FLAG-hFBXL3/p3×FLAG-CMV-10, FLAG-hBMAL1/p3×FLAG-CMV-10, FLAG-hCLOCK/p3×FLAG-CMV-10, hCRY2-WT-LUC/p3×FLAG-CMV-10, hCRY2-A260T-LUC/p3×FLAG-CMV-10, hCRY2-A260D-LUC/p3×FLAG-CMV-10, m*Per1-luc*/pGL3, pRL-TK (Renilla luc expression for internal control in luciferase assay, Promega).

574 0.3kb-m*Bmal1*-luc/pGL3 is a gift by Dr.Yoshitaka Fukada (University of Tokyo).
575 Mutant hCRY2 and hCRY1 expression vectors were generated by PCR-based
576 site-directed mutagenesis, and the mutation was verified by sequencing. For
577 knockdown of human *FBXL3*, Hs_FBXL3_1, Hs_FBXL3_2 FlexiTube siRNA
578 (QIAGEN) and control siRNA (QIAGEN) were purchased.
579
580 **Bioluminescence rhythms in tissue culture**
581 h*CRY2* transgenic mice were crossed with *mPer2*^{Luc} knock-in mice (Yoo et al.,
582 2004; RRID IMSR_JAX006852). Mice were sacrificed between ZT11 and ZT12.
583 Dissected liver tissues were cultured on Millcell culture membrane
584 (PICMORG50, Millpore) in 35 mm dishes. For recording of lung rhythms,
585 dissected lung tissue was placed in 35 mm dishes without Millcell culture
586 membrane. Recording medium was phenol-red free DMEM (Sigma Aldrich)
587 containing 10mM HEPES-pH7.0, 3.5g/L D-glucose, 0.2 mM luciferin potassium
588 salt, 0.35 g/L sodium bicarbonate, 2% B-27 supplement (Life Technologies), 50
589 U/ml penicillin-streptomycin (Life Technologies). Bioluminescence was
590 continuously recorded in a LumiCycle 32 instrument (Actimetrics, Wilmette, IL).
591 Bioluminescence was detrended by subtracting 24-hr average of
592 bioluminescence using the LumiCycle analysis software. The periods were
593 determined by dampened sine-curve fitting using LumiCycle analysis.
594
595 **Bioluminescence rhythms in cell culture**

For h*CRY2* transgenic/m*Cry2* knockout MEFs and NIH3T3 stable cells, cells were transfected with 500 ng 0.3kbp-m*Bmal1*-luc/pGL3 by Lipofectamine3000 before recordings. Cellular rhythms were synchronized by treatment with 100 nM dexamethasone (DEX) for 2 hours. Medium was changed to the recording medium: phenol-red free DMEM (Sigma Aldrich) containing 10mM HEPES-pH7.0, 3.5g/L D-glucose, 0.1 mM luciferin potassium salt and 50 U/ml penicillin-streptomycin (Life Technology). Bioluminescence recording and data analysis were as described in the methods for “Bioluminescence rhythms in tissue culture”.

Luciferase assay

HEK293 cells were transfected with 50 ng *Per1*-luc expression vector, 25 ng Renilla luc control vector and 2, 5, 10 or 20 ng hCRY2 expression vectors. The luciferase assay was performed with Dual-Luciferase Reporter Assay System (Promega) according to the manufacturer’s protocol. Bioluminescence was detected by Synergy^{TM} H4 Hybrid Multi-Mode Microplate Reader (BioTek). Bioluminescence of Firefly LUC was normalized to bioluminescence of Renilla LUC.

Luciferase-based degradation assay

The hCRY2-LUC fusion protein expressing vector was created by inserting a *CRY2-Luc* cDNA between EcoRI and BamHI sites in the p3×FLAG-CMV-10

vector. HEK293 cells were transfected with 50 ng hCRY2-LUC vectors and cultured for 24 hours. The culture medium was replaced with recording medium [phenol-red free DMEM (Sigma Aldrich) supplemented with 10% fetal bovine serum, 3.5 mg/ml glucose, 50 U/ml penicillin-streptomycin (Life Technologies), 0.05 mM luciferin, and 10 mM HEPES-NaOH; pH 7.0] containing 100 μg/ml cycloheximide (CHX; Santa Cruz Biotechnology Inc.). Luciferase activity of hCRY2-LUC was recorded at 10-min intervals at 37°C with a LumiCycle 32 instrument (Actimetrics). The luminescence signals were fitted to an exponential function to quantify the half-life of CRY2-LUC. KL001 (Cayman Chemical) was diluted in DMSO to a final concentration of 20 mM.

Expression profiles of proteins and genes

Mice were entrained to LD 12:12 for at least 10 days. Mice were transferred to DD, and mice were sacrificed in dim red light on the 2nd day of DD. Liver tissues were collected, followed by nuclear extraction (Yoshitane et al., 2009) and mRNA extraction. Protein levels and mRNA levels were normalized to LaminB levels and *Gapdh* levels, respectively.

Western Blotting

For whole-cell extracts, HEK293 cells were lysed in SDS sample buffer [62.5mM Tris-HCl (pH 6.8), 50mM DTT, 2% SDS, 10% glycerol]. Preparation of the cytosolic and the nuclear fractions of mouse liver was performed as previously

described (Yoshitane et al., 2009). Protein samples were separated by SDS-PAGE. Tissues were transfered to PVDF membranes (Millipore) with blocking in T-TBS [50mM Tris-HCl (pH 7.4), 137mM NaCl, 0.1% Tween 20] containing 1% Skim milk. Primary antibodies were reacted in the blocking solution at 4°C overnight. Then, secondary antibodies were reacted in the blocking solution at RT for 2 hr. Proteins were detected with the Western Lightning Plus ECL (PerkinElmer). Band intensities were determined using Image J software. β-actin and Vinculin were used as loading controls for total cell lysates, and LaminB and TBP were used as nuclear markers. Proteins were detected with the following antibodies: anti-cMyc 9E10 (Santa Cruz, sc-40), anti-FLAG M2 (Sigma Aldrich, F1804), anti-HA Y11 (Santa Cruz, sc-805-G), anti-β-actin (Abcam, AC-15), anti-Vinculin (Abcam, ab18058), anti-TBP (Santa Cruz, sc-273), anti-Ub (Santa Cruz, sc-8017), anti-hPER1 (Thermo Scientific, PA1-524), anti-LaminB1 (Abcam, ab16048 and Santa Cruz, C20), anti-mPER2 (Alpha Diagnostic International, PER-21A), anti-hCRY2 (Santa Cruz, sc-130731) and anti-mCRY1 (MBL, PM081). Rabbit polyclonal anti-mCRY2 antibody was provide by Dr.Yoshitaka Fukada (University of Tokyo)(Hirano et al., 2013). Secondary antibodies used were goat anti-mouse IgG-HRP (Santa Cruz, sc-2005), goat anti-rabbit IgG-HRP (Santa Cruz, sc-2006) and goat anti-guinea pig IgG-HRP (Santa Cruz, sc2438).

FAD competition assay

Flavin adenine dinucleotide disodium salt hydrate (FAD, Sigma Aldrich) was diluted in PBS to a final concentration of 100 mM. HEK293 cells were transfected with plasmid vectors for 10 μg hCRY2-His-Myc (WT or A260T) and 10 μg FLAG-hFBXL3. Forty-two hours after transfection, the cells were treated with 10 μM MG132 (Calbiochem) for 6 hours. CRY2-FBXL3 complex was purified with anti-FLAG M2 affinity gel (Sigma Aldrich). FAD was incubated with CRY2-FBXL3 complex binding to anti-FLAG M2 affinity gel in 40 μl PBS for 2 hours on ice. After centrifugation, the supernatant was collected as the 'released CRY2' sample. CRY2 still binding to FLAG-FBXL3 was eluted by adding SDS sample buffer to FLAG-M2 affinity gel.

Immunoprecipitation

HEK293 cells were transfected with plasmid vectors for hCRY2-His-Myc (WT or A260T) and FLAG-hFBXL3. Forty-two hours after transfection, the cells were treated with 10 μM MG132 (Calbiochem) for 6 hours. CRY2-FBXL3 complex was purified with anti-FLAG M2 affinity gel (Sigma Aldrich) and eluted by 300 μg/ml 3×FLAG peptide (Sigma Aldrich).

Real-time qPCR

Total RNA was extracted by TRIzol reagent (Life Technologies) from MEFs or liver samples of transgenic animals. cDNA was synthesized by Superscript III (Life Technologies) for MEFs or GoScript (Promega) for liver samples.

Quantification of mRNA was performed with GoTaq Real-Time qPCR Kits (Promega) using gene specific primers. mRNA levels were normalized to mouse *Gapdh* levels.

Primers: mouse *Per1*-fw; CAGGCTAACCAGGAATATTACCAGC,

mouse *Per1*-rv; CACAGCCACAGAGAAGGTGTCCTGG,

mouse *Per2*-fw; ATGCTCGCCATCCACAAGA,

mouse *Per2*-rv; GCGGAATCGAATGGGAGAAT,

mouse *Gapdh*-fw; ACGGGAAGCTCACTGGCATGGCCTT,

mouse *Gapdh*-rv; CATGAGGTCCACCACCCTGTTGCTG,

mouse *Cry2*-fw; GGGACTCTGTCTATTGGCATCTG,

mouse *Cry2*-rv; GTCACTCTAGCCCGCTTGGT,

mouse *Cry1*-fw:CCCAGGCTTTTCAAGGAATGGAACA

mouse *Cry1*-rv:TCTCATCATGGTCATCAGACAGAGG

human *CRY2*-fw; CCAAGAGGGAAGGGCAGGGTAGAG,

human *CRY2*-rv; AGGATTTGAGGCACTGTTCCGAGG

mouse *Dbp* FW,AATGACCTTTGAACCTGATCCCGCT

mouse *Dbp* RV,GCTCCAGTACTTCTCATCCTTCTGT

mouse *Bmal1* FW,GCAGTGCCACTGACTACCAAGA

mouse *Bmal1* RV,TCCTGGACATTGCATTGCAT

mouse *Rev-erb*α FW,GGGCACAAGCAACATTACCA

mouse *Rev-erb*α RV,CACGTCCCCACACACCTTAC

mouse *REV-erb*β FW,TGGGACTTTTGAGGTTTTAATGG

mouse *REV-erbβ* RV,GTGACAGTCCGTTCCTTTGC

mouse *Dec1* FW,ATCAGCCTCCTTTTTGCCTTC

mouse *Dec1* RV,AGCATTTCTCCAGCATAGGCAG

mouse *Dec2* FW,ATTGCTTTACAGAATGGGGAGCG

mouse *Dec2* RV,AAAGCGCGCGAGGTATTGCAAGAC

Structural modeling

Structural modeling was based on the structure of mouse CRY2 bound to FAD (PDB code 4I6G) and mouse FBXL3 (PDB code 4I6J)(Xing et al., 2013). Modeling of mutant CRY2 was performed using Molecular graphics and analyses were performed with the UCSF Chimera package (RRID SCR_004097). Chimera was developed by the Resource for Biocomputing, Visualization, and Informatics at the University of California, San Francisco (supported by NIGMS P41-GM103311)(Pettersen et al., 2004).

Statistics analysis

All error bars in the figures represent SEM except for Figure 3C. In Figure 3C, the error bars represent SD. No statistical analysis was used to predetermine the sample sizes. Experiments were not randomized and not analyzed blindly. In Figure 2A and Figure 2-supplement 1, the sample with extremely abnormal walking distance (>500 meter walking distance, due to a failure of automatic video tracking) was excluded as an outlier according to the Smirnov-Grubbs test.

Data was statistically analyzed using R software (RRID SCR_001905). To assess statistical significance, data was obtained from three or more independent experiments. All data sets were assumed to follow normal distributions by the Kolmogorov-Smirnov test, and homogeneity of variance between compared groups was tested by F-test (comparison of 2 groups) or Bartlett test (comparison of multiple groups). Two-tailed paired Student's *t*-test or Welch's *t*-test was used for the comparison of 2 groups with or without homogeneity of variance. Tukey's test or Games-Howell test were used for multiple comparisons with or without of homogeneity of variance. Differences with a P value <0.05 were considered statistically significant.

Acknowledgements

This work was funded by NIH grant GM079180 and HL059596 to L.J.P. and Y-H.F and by the William Bowes Neurogenetics Fund. The initial sequencing and analysis were performed at Lawrence Berkeley National Laboratory and at the United States Department of Energy Joint Genome Institute (Department of Energy Contract DE-AC02-05CH11231, University of California). The authors wish to thank Drs. Philip Kurien and Pei-Ken Hsu and Mr. David Wu for suggestions and critical reading of the manuscript. We thank Dr. Yoshitaka Fukada (University of Tokyo) for providing anti-CRY2 antibody and 0.3 kbp-m*Bmal1*-luc construct. L.J.P. is an investigator of the Howard Hughes Medical Institute. A.H. was supported by the Japanese Society for the Promotion

of Science (JSPS) and the Uehara Memorial Foundation (Japan).

Additional Information

Author Contributions

C.R.J carried out human circadian evaluations. A.L. and L.A.P. performed initial genomic sequencing and analysis. G.S. and Y. X. generated the BAC transgenic mouse models. W.C.H. performed structural modeling. A.H., T.M. and M.Y. performed experiments. A.H, Y.-H.F, and L.J.P designed experiments, analyzed data and wrote the manuscript.

References

Burgess, H.J., and Fogg, L.F. (2008). Individual differences in the amount and timing of salivary melatonin secretion. PLoS ONE *3*, e3055.

Busino, L., Bassermann, F., Maiolica, A., Lee, C., Nolan, P.M., Godinho, S.I., Draetta, G.F., and Pagano, M. (2007). SCFFbxl3 controls the oscillation of the circadian clock by directing the degradation of cryptochrome proteins. Science *316*, 900–904.

Czarna, A., Berndt, A., Singh, H.R., Grudziecki, A., Ladurner, A.G., Timinszky, G., Kramer, A., and Wolf, E. (2013). Structures of Drosophila Cryptochrome and Mouse Cryptochrome1 Provide Insight into Circadian Function. Cell *153*, 1394–1405.

Dupuis, J., Langenberg, C., Prokopenko, I., Saxena, R., Soranzo, N., Jackson, A.U., Wheeler, E., Glazer, N.L., Bouatia-Naji, N., Gloyn, A.L., et al. (2010). New genetic loci implicated in fasting glucose homeostasis and their impact on type 2 diabetes risk. Nat Genet *42*, 105–116.

775 Godinho, S.I.H., Maywood, E.S., Shaw, L., Tucci, V., Barnard, A.R., Busino, L.,
776 Pagano, M., Kendall, R., Quwailid, M.M., Romero, M.R., et al. (2007). The
777 after-hours mutant reveals a role for Fbxl3 in determining mammalian circadian
778 period. Science *316*, 897–900.

779 Griffin, E.A., Staknis, D., and Weitz, C.J. (1999). Light-independent role of CRY1
780 and CRY2 in the mammalian circadian clock. Science *286*, 768–771.

781 Guilding, C., Scott, F., Bechtold, D.A., Brown, T.M., Wegner, S., and Piggins,
782 H.D. (2013). Suppressed cellular oscillations in after-hours mutant mice are
783 associated with enhanced circadian phase-resetting. The Journal of Physiology
784 *591*, 1063–1080.

785 He, Y., Jones, C.R., Fujiki, N., Xu, Y., Guo, B., Holder, J.L., Rossner, M.J.,
786 Nishino, S., and Fu, Y.H. (2009). The Transcriptional Repressor DEC2
787 Regulates Sleep Length in Mammals. Science *325*, 866–870.

788 Hirano, A., Kurabayashi, N., Nakagawa, T., Shioi, G., Todo, T., Hirota, T., and
789 Fukada, Y. (2014). In Vivo Role of Phosphorylation of Cryptochrome 2 in the
790 Mouse Circadian Clock. Molecular and Cellular Biology *34*, 4464–4473.

791 Hirano, A., Yumimoto, K., Tsunematsu, R., Matsumoto, M., Oyama, M.,
792 Kozuka-Hata, H., Nakagawa, T., Lanjakornsiripan, D., Nakayama, K.I., and
793 Fukada, Y. (2013). FBXL21 Regulates Oscillation of the Circadian Clock through
794 Ubiquitination and Stabilization of Cryptochromes. Cell *152*, 1106–1118.

795 Hirota, T., Lee, J.W., St John, P.C., Sawa, M., Iwaisako, K., Noguchi, T.,
796 Pongsawakul, P.Y., Sonntag, T., Welsh, D.K., Brenner, D.A., et al. (2012).
797 Identification of Small Molecule Activators of Cryptochrome. Science *337*, 1094–
798 1097.

799 Hitomi, K., DiTacchio, L., Arvai, A.S., Yamamoto, J., Kim, S.-T., Todo, T., Tainer,
800 J.A., Iwai, S., Panda, S., and Getzoff, E.D. (2009). Functional motifs in the (6-4)
801 photolyase crystal structure make a comparative framework for DNA repair

photolyases and clock cryptochromes. Proc Natl Acad Sci U S a. *106*, 6962–6967.

Hoffman, A.E., Zheng, T., Yi, C.H., Stevens, R.G., Ba, Y., Zhang, Y., Leaderer, D., Holford, T., Hansen, J., and Zhu, Y. (2010). The Core Circadian Gene Cryptochrome 2 Influences Breast Cancer Risk, Possibly by Mediating Hormone Signaling. Cancer Prevention Research *3*, 539–548.

Jones, C.R., Campbell, S.S., Zone, S.E., Cooper, F., DeSano, A., Murphy, P.J., Jones, B., Czajkowski, L., and Ptáček, L.J. (1999). Familial advanced sleep-phase syndrome: A short-period circadian rhythm variant in humans. Nature Medicine *5*, 1062–1065.

Kaasik, K., Kivimäe, S., Allen, J.J., Chalkley, R.J., Huang, Y., Baer, K., Kissel, H., Burlingame, A.L., Shokat, K.M., Ptáček, L.J., et al. (2013). Glucose Sensor O-GlcNAcylation Coordinates with Phosphorylation to Regulate Circadian Clock. Cell Metabolism *17*, 291–302.

Kovanen, L., Kaunisto, M., Donner, K., Saarikoski, S.T., and Partonen, T. (2013). CRY2 genetic variants associate with dysthymia. PLoS ONE *8*, e71450.

Kume, K., Zylka, M.J., Sriram, S., Shearman, L.P., Weaver, D.R., Jin, X., Maywood, E.S., Hastings, M.H., and Reppert, S.M. (1999). mCRY1 and mCRY2 Are Essential Components of the Negative Limbof the Circadian Clock Feedback Loop. Cell *98*, 193–205.

Lavebratt, C., Sjöholm, L.K., Soronen, P., Paunio, T., Vawter, M.P., Bunney, W.E., Adolfsson, R., Forsell, Y., Wu, J.C., Kelsoe, J.R., et al. (2010). CRY2 is associated with depression. PLoS ONE *5*, e9407.

Lee, H.-Y., Nakayama, J., Xu, Y., Fan, X., Karouani, M., Shen, Y., Pothos, E.N., Hess, E.J., Fu, Y.-H., Edwards, R.H., et al. (2012). Dopamine dysregulation in a mouse model of paroxysmal nonkinesigenic dyskinesia. J. Clin. Invest. *122*, 507–518.

Lin, C., and Todo, T. (2005). The cryptochromes. Genome Biol. *6*, 220.

Lowrey, P.L., and Takahashi, J.S. (2004). Mammalian circadian biology: elucidating genome-wide levels of temporal organization. Annu Rev Genomics Hum Genet *5*, 407–441.

Lowrey, P.L., Shimomura, K., Antoch, M.P., Yamazaki, S., Zemenides, P.D., Ralph, M.R., Menaker, M., and Takahashi, J.S. (2000). Positional syntenic cloning and functional characterization of the mammalian circadian mutation tau. Science *288*, 483–491.

Nangle, S., Xing, W., and Zheng, N. (2013). Crystal structure of mammalian cryptochrome in complex with a small molecule competitor of its ubiquitin ligase. Cell Research *23*, 1417–1419.

Okamura, H., Okamura, H., Miyake, S., Sumi, Y., Yamaguchi, S., Yasui, A., Muijtjens, M., Hoeijmakers, J.H.J., and van der Horst, G.T.J. (1999). Photic Induction of mPer1 and mPer2 in Cry-Deficient Mice Lacking a Biological Clock. Science *286*, 2531–2534.

Parsons, M.J., Lester, K.J., Barclay, N.L., Archer, S.N., Nolan, P.M., Eley, T.C., and Gregory, A.M. (2014). Polymorphisms in the circadian expressed genes PER3and ARNTL2are associated with diurnal preference and GNβ3with sleep measures. J Sleep Res *23*, 595–604.

Partch, C.L., and Sancar, A. (2005). Cryptochromes and Circadian Photoreception in Animals. Methods in Enzymology *393*, 726–745.

Pettersen, E.F., Goddard, T.D., Huang, C.C., Couch, G.S., Greenblatt, D.M., Meng, E.C., and Ferrin, T.E. (2004). UCSF Chimera--a visualization system for exploratory research and analysis. J Comput Chem *25*, 1605–1612.

Reid, K.J., and Burgess, H.J. (2005). Circadian Rhythm Sleep Disorders. Primary Care: Clinics in Office Practice *32*, 449–473.

Reid, K.J., Chang, A.-M., Dubocovich, M.L., Turek, F.W., Takahashi, J.S., and Zee, P.C. (2001). Familial advanced sleep phase syndrome. Arch Neurol *58*, 1089–1094.

Reischl, S., and Kramer, A. (2011). Kinases and phosphatases in the mammalian circadian clock. FEBS Letters *585*, 1393–1399.

Reppert, S.M., and Weaver, D.R. (2001). MOLECULAR ANALYSIS OF MAMMALIAN CIRCADIAN RHYTHMS. Annu. Rev. Physiol *63*, 647–676.

Roenneberg, T., Kuehnle, T., Pramstaller, P.P., Ricken, J., Havel, M., Guth, A., and Merrow, M. (2004). A marker for the end of adolescence. Curr Biol *14*, R1038–R1039.

Sanada, K., Harada, Y., Sakai, M., Todo, T., and Fukada, Y. (2004). Serine phosphorylation of mCRY1 and mCRY2 by mitogen-activated protein kinase. Genes Cells *9*, 697–708.

Shearman, L.P., Sriram, S., Weaver, D.R., Maywood, E.S., Chaves, I., Zheng, B., Kume, K., Lee, C.C., Hastings, M.H., and Reppert, S.M. (2000). Interacting molecular loops in the mammalian circadian clock. Science *288*, 1013–1019.

Shi, G., Xing, L., Liu, Z., Qu, Z., Wu, X., Dong, Z., Wang, X., Gao, X., Huang, M., Yan, J., et al. (2013). Dual roles of FBXL3 in the mammalian circadian feedback loops are important for period determination and robustness of the clock. Proc Natl Acad Sci U S a. *110*, 4750–4755.

Siepka, S.M., Yoo, S.-H., Park, J., Song, W., Kumar, V., Hu, Y., Lee, C., and Takahashi, J.S. (2007). Circadian mutant Overtime reveals F-box protein FBXL3 regulation of cryptochrome and period gene expression. Cell *129*, 1011–1023.

Sjöholm, L.K., Backlund, L., Cheteh, E.H., Ek, I.R., Frisén, L., Schalling, M., Osby, U., Lavebratt, C., and Nikamo, P. (2010). CRY2 is associated with rapid cycling in bipolar disorder patients. PLoS ONE *5*, e12632.

St John, P.C., Hirota, T., Kay, S.A., and Doyle, F.J. (2014). Spatiotemporal separation of PER and CRY posttranslational regulation in the mammalian circadian clock. Proc Natl Acad Sci U S a. *111*, 2040–2045.

884 Stojkovic, K., Wing, S.S., and Cermakian, N. (2014). A central role for
885 ubiquitination within a circadian clock protein modification code. Front Mol
886 Neurosci *7*, 69.

887 Takahashi, J.S. (1995). Molecular neurobiology and genetics of circadian
888 rhythms in mammals. Annu. Rev. Neurosci. *18*, 531–553.

889 Toh, K.L., Jones, C.R., He, Y., Eide, E.J., Hinz, W.A., Virshup, D.M., Ptáček, L.J.,
890 and Fu, Y.-H. (2001). An hPer2 phosphorylation site mutation in familial
891 advanced sleep phase syndrome. Science *291*, 1040–1043.

892 van der Horst, G.T.J., Muijtjens, M., Kobayashi, K., Takano, R., Kanno, S.-I.,
893 Takao, M., de Wit, J., Verkerk, A., Eker, A.P.M., van Leenen, D., et al. (1999).
894 Mammalian Cry1 and Cry2 are essential for maintenance of circadian rhythms.
895 Nature *398*, 627–630.

896 Vitaterna, M.H., Selby, C.P., Todo, T., Niwa, H., Thompson, C., Fruechte, E.M.,
897 Hitomi, K., Thresher, R.J., Ishikawa, T., Miyazaki, J., et al. (1999). Differential
898 regulation of mammalian period genes and circadian rhythmicity by
899 cryptochromes 1 and 2. Proc. Natl. Acad. Sci. U.S.a. *96*, 12114–12119.

900 Xing, W., Busino, L., Hinds, T.R., Marionni, S.T., Saifee, N.H., Bush, M.F.,
901 Pagano, M., and Zheng, N. (2013). SCFFBXL3 ubiquitin ligase targets
902 cryptochromes at their cofactor pocket. Nature *496*, 64–68.

903 Xu, Y., Toh, K.L., Jones, C.R., Shin, J.Y., Fu, Y.H., and Ptáček, L.J. (2007).
904 Modeling of a Human Circadian Mutation Yields Insights into Clock Regulation
905 by PER2. Cell *128*, 59–70.

906 Xu, Y., Padiath, Q.S., Shapiro, R.E., Jones, C.R., Wu, S.C., Saigoh, N., Saigoh,
907 K., Ptáček, L.J., and Fu, Y.-H. (2005). Functional consequences of a CKIdelta
908 mutation causing familial advanced sleep phase syndrome. Nature *434*, 640–
909 644.

910 Yoo, S.-H., Mohawk, J.A., Siepka, S.M., Shan, Y., Huh, S.K., Hong, H.-K.,
911 Kornblum, I., Kumar, V., Koike, N., Xu, M., et al. (2013). Competing E3 ubiquitin

ligases govern circadian periodicity by degradation of CRY in nucleus and cytoplasm. Cell *152*, 1091–1105.

Yoo, S.-H., Yamazaki, S., Lowrey, P.L., Shimomura, K., Ko, C.H., Buhr, E.D., Siepka, S.M., Hong, H.-K., Oh, W.J., Yoo, O.J., et al. (2004). PERIOD2::LUCIFERASE real-time reporting of circadian dynamics reveals persistent circadian oscillations in mouse peripheral tissues. Proc. Natl. Acad. Sci. U.S.a. *101*, 5339–5346.

Yoshitane, H., Takao, T., Satomi, Y., Du, N.H., Okano, T., and Fukada, Y. (2009). Roles of CLOCK Phosphorylation in Suppression of E-Box-Dependent Transcription. Molecular and Cellular Biology *29*, 3675–3686.

Zhang, L., Hirano, A., Hsu, P.-K., Jones, C.R., Sakai, N., Okuro, M., McMahon, T., Yamazaki, M., Xu, Y., Saigoh, N., et al. (2016). A PERIOD3 variant causes a circadian phenotype and is associated with a seasonal mood trait. Proc Natl Acad Sci U S a. *113*, E1536–E1544.

Zhang, L., Ptáček, L.J., and Fu, Y.-H. (2013). Diversity of Human Clock Genotypes and Consequences (Elsevier Inc.).

Figure Legends

Figure 1. **A *CRY2* mutation in FASP kindred 50035.**

(**A**) Pedigree of the family (kindred 50035) segregating the *CRY2* mutation (A260T). Circles and squares represent women and men, respectively. An asterisk marks the proband. A missense mutation from G to A causes an amino acid conversion from Alanine to Threonine at position 260. (**B**) Amino acid alignment around the mutation site. The A260T mutation is located in the N-terminal portion of the FAD binding domain in CRY2. This residue is highly

conserved among vertebrate species. CC denotes a Coiled-Coil sequence.

Figure 2. h*CRY2-A260T* mice have advanced phase of sleep-wake behavior in a light-dark cycle and a shortened circadian period in constant darkness.

(**A**) Mouse movement was tracked by an infrared video camera in LD. The ratio of immobilization time to total daily immobilization time (upper panel) and the ratio of walking distance to total daily distance (bottom panel) were plotted every 10 min. Data are shown as means with SEM (n=8 for h*CRY2-WT* and h*CRY2-A260T*). (**B**) Peak time of immobility was measured by fitting a quadratic function to data from ZT0 to 13. Representative examples of curve fitting for h*CRY2-WT* and h*CRY2-A260T* are shown here. Data are shown as means with SEM (n=8 for h*CRY2-WT* and h*CRY2-A260T*, *p<0.05 by Student's *t*-test). (**C**) Onset and offset of locomotor activity. Data are shown as means with SEM (n=8 for h*CRY2-WT* and h*CRY2-A260T*). (**D**) Actograms of wheel-running activity for *hCRY2-WT*, h*CRY2-A260T*, and littermate transgene-negative mice. The blue shadows indicate periods when the lights were on. Red lines were fitted to activity onset using ClockLab analysis software. (**E**) Phase-shifts in response to a 30-min light exposure at ZT14 indicated by red arrows in (**D**). *p<0.05 by Tukey's test (n=7 for h*CRY2-WT,* n=11 for h*CRY2-A260T,* n=10 for WT). (**F**) The distribution of period measurements for BAC transgenic mice and transgene negative controls. Period was determined by line fitting of activity onset and

chi-square periodogram from day 7 to day 19 in DD. *p<0.05 (n=15 for h*CRY2-WT*, n=14 for h*CRY2-A260T* and n=7 for WT)

Figure 3. Bioluminescence rhythms in tissue cultures from h*CRY2-A260T* mice and *CRY2-A260T* stable cell lines.

(**A**) Representative rhythms of PER2::LUC bioluminescence in the liver and lung. Data were detrended by subtracting the 24-hr average of bioluminescence. (**B**) Period measurements of the bioluminescence rhythms in liver and lung tissues. Data are shown as means ± SEM (n=4 for liver and h*CRY2-WT* lung, n=3 for h*CRY2-A260T* lung, *p<0.05 by Student's *t*-test). (**C**) Peak and trough time of PER2::LUC bioluminescence rhythms of mouse liver and lung tissues. Data are shown as means ± SEM (n=4 for liver). Data are shown as means ± SD (n=2 to 4 for lung, *p<0.05 by Student's *t*-test). (**D**) Representative rhythms of PER2::LUC bioluminescence in MEFs from h*CRY2* transgenic mice. Data were detrended by subtracting the 24-hr average of bioluminescence. Period lengths of the bioluminescence rhythms are shown as means ± SEM (n=4, *p<0.05 by Tukey's test). (**E**) Representative examples of bioluminescence rhythms of m*Bmal1-luc* in MEFs from transgenic mice on a m*Cry2* knockout background. Cells were transfected with m*Bmal1*-luc vector 24 hours before the recording. Data were detrended by subtracting the 24-hr average of bioluminescence. Period lengths of the bioluminescence rhythms in the stable cell lines are shown as means ± SEM (n=4, *p<0.05 by Games-Howell test). (**F**) Representative

examples of bioluminescence rhythms of *Bmal1-luc* in NIH3T3 cells stably expressing FLAG-CRY2-WT or FLAG-CRY2-A260T. Data were detrended by subtracting the 24-hr average of bioluminescence. Period lengths of the bioluminescence rhythms in the stable cell lines are shown as means ± SEM (n=3, *p<0.05 by Student's *t*-test).

Figure 4. CRY2-A260T is less stable, particularly in nuclei.

(**A**) Luciferase activity driven by mouse *Per1* E-box in HEK293 cells. 2, 5, 10 and 20 ng of hCRY2 expression vector (WT or A260T) was transfected into cells cultured in a 24-well plate. Luciferase activity was normalized to Renilla luciferase activity. Data are shown as means with SEM (n=4, *p<0.05 by Student's *t*-test). (**B**) Protein levels of CRY2-WT and CRY2-A260T in the nuclear and cytosolic fractions of HEK293 cells. Data are shown as means with SEM (n=3, *p<0.05 by Student's *t*-test). (**C**) Degradation assay of CRY2 protein in HEK293 cells. Forty-eight hours after transfection, cells were treated with 100 μg/ml CHX and fractionated into the nuclear and cytosolic fractions. CRY2 protein levels at the starting point (t=0 hours) were normalized to 1. Data are shown as means with SEM (n=3*, p<0.05 by Student's *t*-test).

Figure 5. CRY2-A260T binds more strongly to FBXL3 leading to faster degradation of mutant CRY2.

(**A**) Effect of human *FBXL3* knockdown on CRY2 protein stability in HEK293

cells. Forty-eight hours after transfection, the culture medium was changed to the recording medium containing 100 μg/ml CHX, and bioluminescence of CRY2-LUC was recorded continuously. Bioluminescence normalized to the value at time 0 was fitted to an exponential curve to determine half-life of CRY2-LUC. Data are shown as means with SEM (n=4, *p<0.05 by Welch's *t*-test). (**B**) Effect of FAD on CRY2 protein levels. Forty-two hours after transfection, HEK293 cells were treated with 100 μM FAD for 6 hours. Data are shown as means with SEM (n=3, *p<0.05 by Student's *t*-test). (**C**) FAD and FBXL3 competition assay. CRY2-FBXL3 complex expressed in HEK293 cells was purified using FLAG antibody. FAD was added to CRY2-FBXL3 complex and incubated at 4 °C for 2 hours *in vitro*. (**D**) CRY2 protein stability in the cells treated with KL001. Twenty-four hours after transfection, the culture medium was changed to the recording medium containing 100 μg/ml CHX and KL001. Recording of bioluminescence and calculation of half-life was performed as described above. *p<0.05 by Student's *t*-test (n=3). (**E**) Interaction of CRY2 with FBXL3 in HEK293 cells treated with MG132 for 6 hours prior to harvesting. (**F**) Ubiquitylation of CRY2. HEK293 cells expressing FLAG-CRY2 were treated with MG132 for 6 hours before harvesting. FLAG-CRY2 was then purified and blotted with anti-Ubiquitin antibody. Quantitative data are shown as means with SEM (n=3, *p<0.05 by Student's *t*-test).

Figure 6. CRY2-A260T expression is down-regulated in h*CRY2-A260T*

mice.

(**A**) CRY2 protein levels in synchronized MEFs. Cells were treated with 100 nM Dex for 2 hours to synchronize the cellular rhythms. Media was change and MEFs were cultured for 24 or 36 hours before harvesting. Quantified band intensities of CRY2 (mouse CRY2 and human CRY2) are shown as means ± SEM (n=3, *p<0.05 by Student's *t*-test). (**B**) mRNA levels of clock genes in synchronized MEFs. Cellular rhythms of MEFs were synchronized with 100 nM Dex for 2 hours. mRNA levels were quantified by real-time PCR. Data are shown as means ± SEM (n=3, *p<0.05 by Student's *t*-test). (**C**) Temporal expression profiles of PER1, PER2, CRY1 and CRY2 in mouse liver. Mice were sacrificed every 4 hours on the second day in DD. Asterisks mark non-specific bands. (**D**) Quantification of protein levels in (**C**). Data are shown as means ± SEM (n=3). (**E**) mRNA levels of indicated clock genes in mouse liver. Mice were sacrificed every 4 hours on the second day in DD. mRNA levels of indicated genes were quantified by real-time PCR using gene specific primers. Data are shown as means ± SEM (n=3). (**F**) Model of CRY2 protein regulation. In wild-type, FAD binding to CRY2 acts to stabilize by competing with FBXL3. In h*CRY2-A260T* transgenic mice or FASP human subjects with CRY2 mutations, FAD does not protect CRY2 from FBXL3-mediated degradation. Destabilization of CRY2 results in shortened period, leading to advanced sleep phase. In *Fbxl3* knockout mice or mutant mice (*Overtime* and *After-hours*)(Godinho et al., 2007; Siepka et al., 2007), CRY2 is stabilized in the nucleus, thus lengthening the circadian

period.

Figure 1-source data 1

Summary of sleep phenotype of human subjects. Subject IDs correspondence to numbers in Figure 1A.

Figure 2-supplement 1

(**A**) CRY2 expression in total liver lysate at ZT18. CRY2 protein was detected by human CRY2 antibody (Santa Cruz) and mouse CRY2 antibody (Hirano et al., 2013). Copy number was determined by real-time PCR using common sequences in mouse and human *Cry2* genes. (**B**) Representative profiles of locomotor activity measured by video recording. Activity onset (black) and offset (red) are indicated by arrows in the figures. The time of onset and offset for all animals of respective genotypes are averaged and plotted in Figure2C. (**C**) Locomotor activity and resting behavior of transgenic mice on a m*Cry2* knockout background. Mouse movement was tracked by an infrared video camera in LD. The ratio of immobilization time to total daily immobilization time (upper panel) and the ratio of walking distance to total daily distance (bottom panel) were plotted every 10 min. Data are shown as means with SEM (n=6 for h*CRY2-WT*/*Cry2* KO, n=6 for h*CRY2-A260T*/*Cry2* KO). The average of activity offset and onset in LD 12:12 are shown (n=6 for h*CRY2-WT*/*Cry2* KO, n=6 for h*CRY2-A260T*/*Cry2* KO).

Figure 2-supplement 2

(**A**) Activity profiles of transgenic mice in LD 12:12. Ratio of wheel-running counts to total daily counts are plotted every 20 min (n=18 for h*CRY2-WT*, n=14 for h*CRY2-A260T*). The average of activity offset in LD 12:12 are shown in the right graph. *p<0.05 by Tukey's test (n=19 for h*CRY2-WT*, n=19 for h*CRY2-A260T* and n=7 for WT). (**B**) Actograms and activity profiles of transgenic mice on a m*Cry2* knockout background in LD 12:12. Ratio of wheel-running counts to total daily counts are plotted every 5 min (n=5 for h*CRY2-WT*, n=5 for h*CRY2-A260T*). The average of activity offset in LD 12:12 are shown in the right graph. *p<0.05 by Tukey's test (n=5 for h*CRY2-WT*/m*Cry2* KO, n=5 for h*CRY2-A260T*/m*Cry2* KO and n=6 for m*Cry2* KO).

Figure 2-supplement 3

(**A**) Phase-shift in response to 30-min light exposure at ZT22. Mice were exposed to a 30-min light pulse at ZT22 (indicated by red arrows) and released into DD after the light pulse. The blue shadows indicate periods when the lights were on. Red lines were fitted to activity onset using ClockLab analysis software. Phase-shift was determined by line-fitting to activity onset (n=6 for h*CRY2-WT*, n=7 for h*CRY2-A260T* and WT).

Figure 2-supplement 4

(**A**) Circadian period of the transgenic mice on a m*Cry2* knockout background. Period was determined by chi-square periodgram from day 7 to day 14 in DD. *p<0.05 by Welch's test (n=6 for h*CRY2-WT*/m*Cry2*KO and n=5 for h*CRY2-A260T*/m*Cry2*KO). (**B**) Circadian period and phase-shift of h*CRY2-A260T* mice line#2. Representative actograms of wheel-running activity of h*CRY2-A260T* line#2 and littermate controls (*WT*) are shown. The blue shadows indicate periods when the lights were on. Red lines were fitted to activity onset using ClockLab analysis software. Phase-shifts shown here are by 30-min light exposure at ZT14 (left panel, n=7 for h*CRY2-A260T* line#2, n=3 for *WT*). Period was determined by line fitting of activity onset from day 7 to day 19 in DD. *p<0.05 by Student's *t*-test (right panel, n=7 for h*CRY2-A260T* line#2, n=3 for *WT*).

Figure 4-supplement 1

(**A**) Twenty-four hours after transfection, the culture media was changed to recording media containing 100 μg/ml CHX, and bioluminescence of CRY2-LUC (WT, A260T or A260D) was recorded continuously. Bioluminescence normalized to the start point was fitted to an exponential curve to determine half-life of CRY2-LUC (right panel). Data are shown as means ± SEM (n=4, *p<0.05 by Tukey's test). Left panel shows representative bioluminescence decay of CRY2-LUC. (**B**) Luciferase activity driven by mouse *Per1* E-box. 10 or 25 ng of

CRY2 construct was transfected to HEK293 cells cultured in 24-well plate. Luciferase activity was normalized to Renilla luciferase activity. Data are shown as means ± SEM (n=3, *p<0.05 by Tukey's test). (**C**) Degradation assay of CRY1 protein in HEK293 cells. Sixty hours after transfection, cells were treated with 100 μg/ml CHX and fractionated into the nuclear and cytosolic fractions. CRY1 protein levels at the starting point (t=0 hours) were normalized to 1. Data are shown as means with SEM (n=3*, p<0.05 by Student's *t*-test).

Figure 5-supplement 1

(**A**) CRY2 protein stability in the cells treated with KL001. Twenty-four hours after transfection, the culture medium was changed to the recording medium containing 100 μg/ml CHX and KL001 at the indicated concentration. *p<0.05 by Student's *t*-test (n=3). (**B**) Structure of mouse CRY2 bound to FAD (PDB code 4I6G) (orange) or FBXL3 (4I6J) (red). Green represents FBXL3. Short dashed lines indicate the side chain of A259 (A260 of human CRY2). CRY2 bound to FBXL3 is in a more open conformation compared to the FAD-bound CRY2.
(**C**) Structure of mouse CRY2-WT (top) or mouse CRY2-A259T (corresponded to human CRY2-A260T, bottom) bound to FBXL3. The Ala to Thr mutation increases the molecular density and likely changes the conformation of CRY2 from the FAD-bound form to the FBXL3-bound form, in which main chain around A259 moved to left side in this image.

Figure 6-supplement 1

(**A**) mRNA levels of indicated genes in synchronized MEFs. Cellular rhythms of MEFs were synchronized with 100 nM Dex for 2 hours. mRNA levels were quantified by real-time PCR. Data are shown as means ± SEM (n=3, *p<0.05 by Student's *t*-test). (**B**) Expression patterns of indicated clock genes in mouse liver. Mice were sacrificed every 4 hours on the second day in DD. mRNA levels of indicated genes were quantified by real-time PCR using gene specific primers. Data are shown as means ± SEM (n=3).

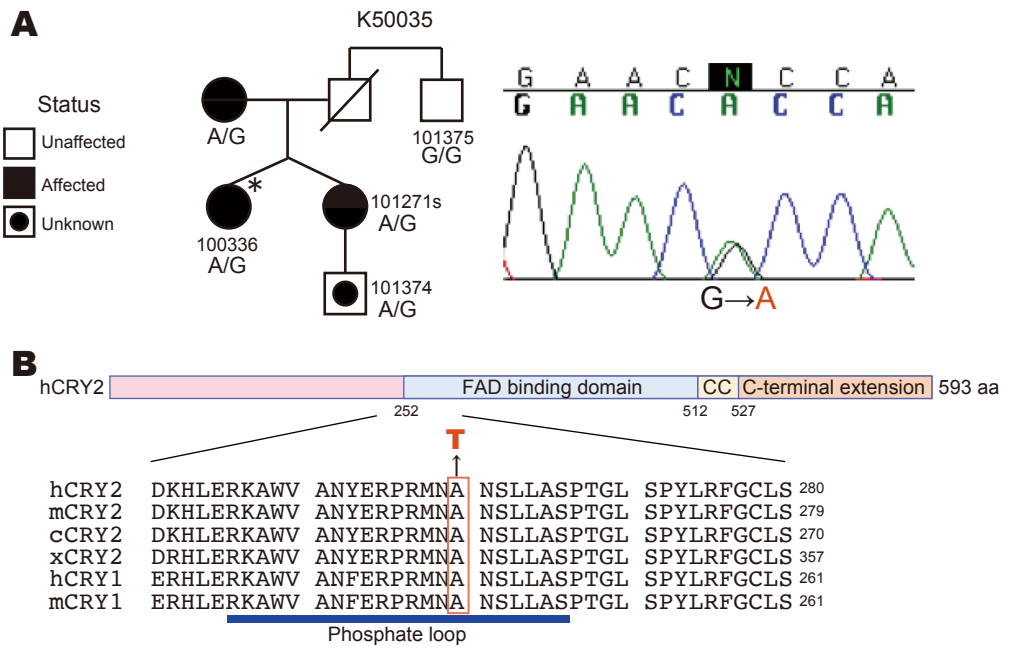
A
K50035
Status
Unaffected
Affected
Unknown
A/G
101375
G/G
*
100336
A/G
101271s
A/G
101374
A/G
G A A C N C C A
G A A C A C C A
G→A
B
hCRY2
FAD binding domain
CC
C-terminal extension
593 aa
252
512
527
T
hCRY2 DKHLERKAWV ANYERPRMNA NSLLASPTGL SPYLRFGCLS 280
mCRY2 DKHLERKAWV ANYERPRMNA NSLLASPTGL SPYLRFGCLS 279
cCRY2 DKHLERKAWV ANYERPRMNA NSLLASPTGL SPYLRFGCLS 270
xCRY2 DRHLERKAWV ANYERPRMNA NSLLASPTGL SPYLRFGCLS 357
hCRY1 ERHLERKAWV ANFERPRMNA NSLLASPTGL SPYLRFGCLS 261
mCRY1 ERHLERKAWV ANFERPRMNA NSLLASPTGL SPYLRFGCLS 261
Phosphate loop

Figure 1

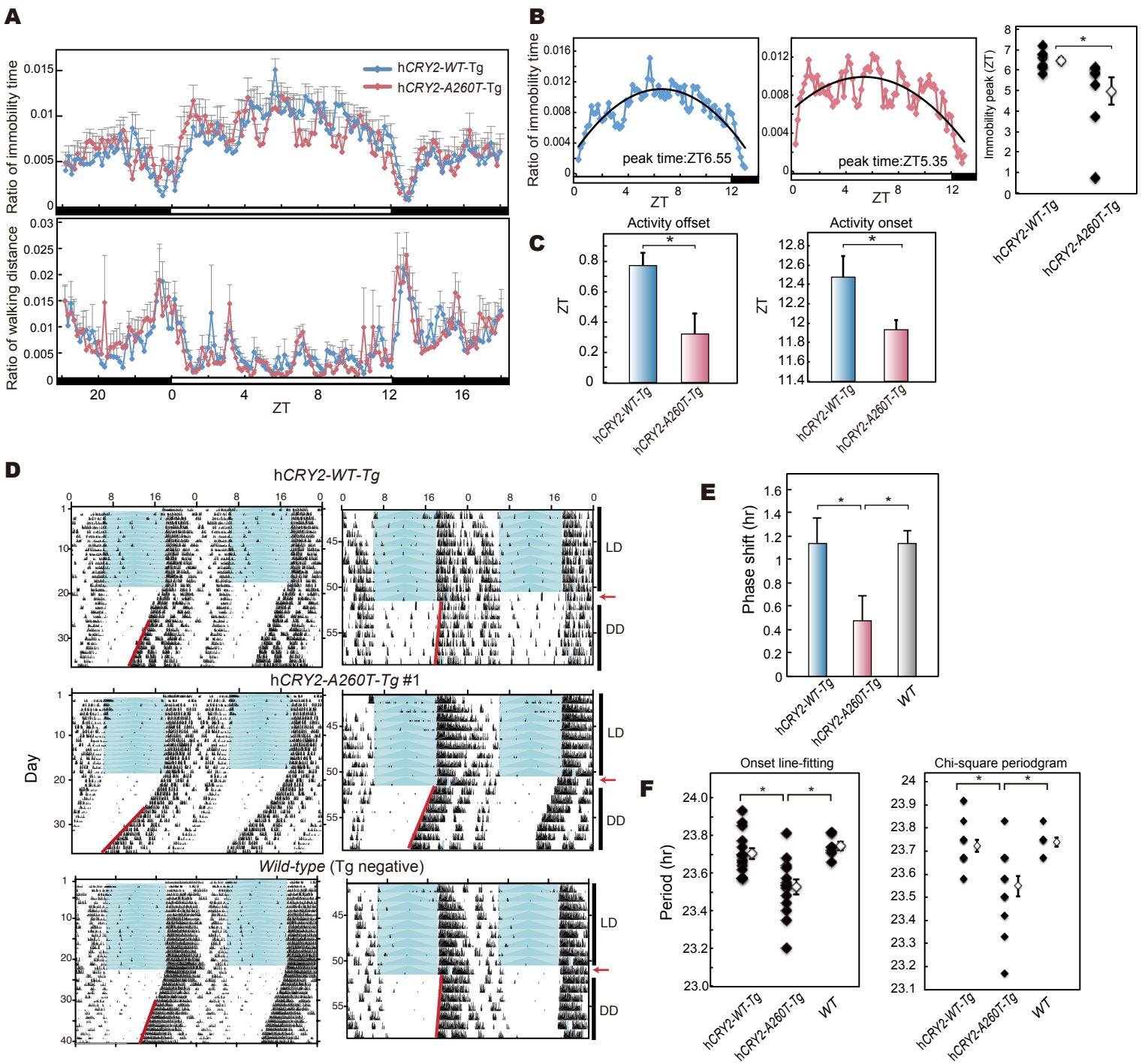
A
Ratio of immobility time
hCRY2-WT-Tg
hCRY2-A260T-Tg
Ratio of walking distance
ZT
B
Ratio of immobility time
peak time:ZT6.55
peak time:ZT5.35
ZT
Immobility peak (ZT)
hCRY2-WT-Tg
hCRY2-A260T-Tg
C
Activity offset
Activity onset
ZT
hCRY2-WT-Tg
hCRY2-A260T-Tg
D
hCRY2-WT-Tg
hCRY2-A260T-Tg #1
Wild-type (Tg negative)
Day
LD
DD
E
Phase shift (hr)
hCRY2-WT-Tg
hCRY2-A260T-Tg
WT
F
Onset line-fitting
Chi-square periodgram
Period (hr)
hCRY2-WT-Tg
hCRY2-A260T-Tg
WT

Figure 2

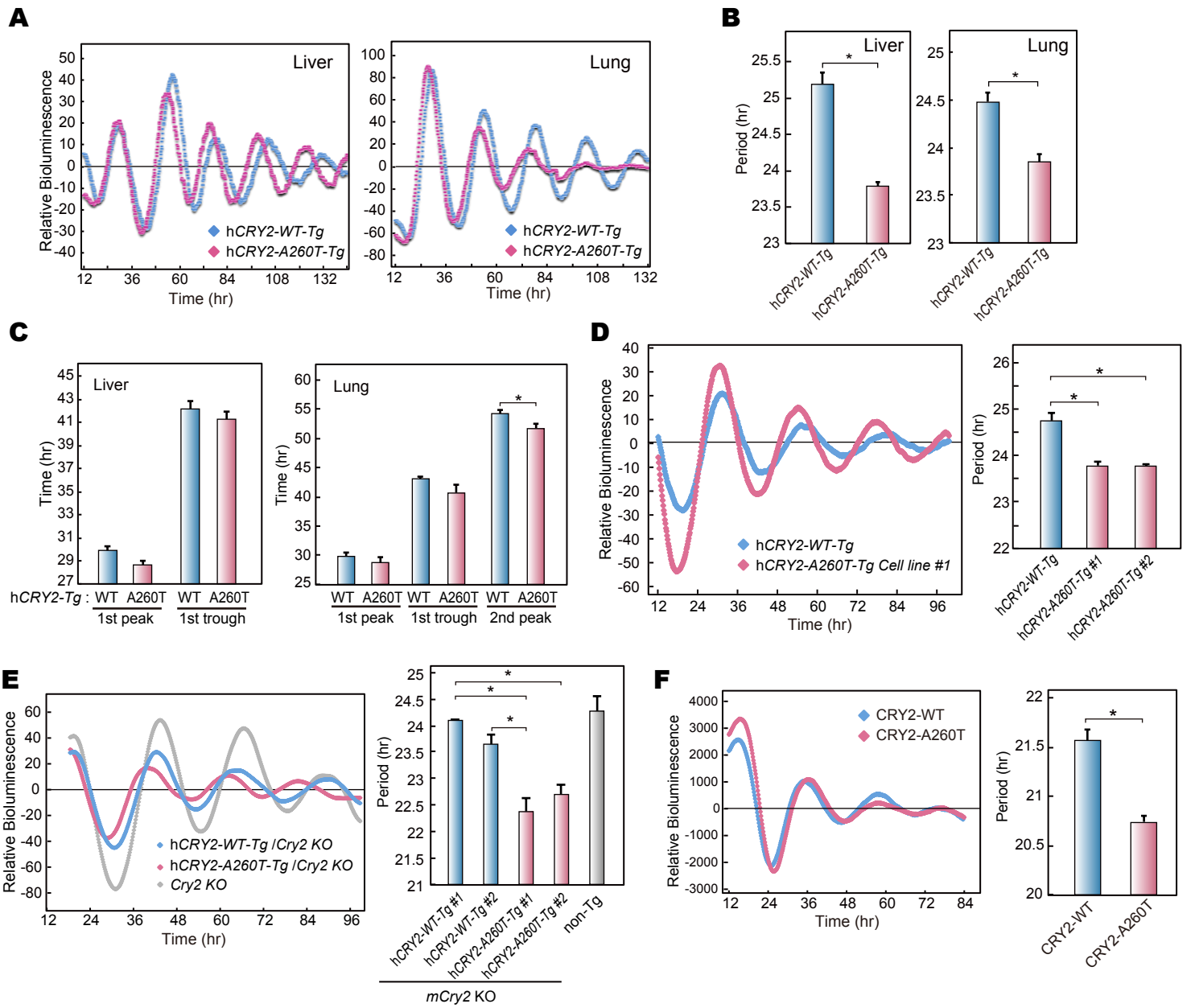
A
Liver
Lung
Relative Bioluminescence
Time (hr)
hCRY2-WT-Tg
hCRY2-A260T-Tg
B
Liver
Lung
Period (hr)
hCRY2-WT-Tg
hCRY2-A260T-Tg
C
Liver
Lung
Time (hr)
hCRY2-Tg : WT A260T WT A260T
1st peak
1st trough
WT A260T WT A260T WT A260T
1st peak
1st trough
2nd peak
D
Relative Bioluminescence
Time (hr)
hCRY2-WT-Tg
hCRY2-A260T-Tg Cell line #1
Period (hr)
hCRY2-WT-Tg
hCRY2-A260T-Tg #1
hCRY2-A260T-Tg #2
E
Relative Bioluminescence
Time (hr)
hCRY2-WT-Tg /Cry2 KO
hCRY2-A260T-Tg /Cry2 KO
Cry2 KO
Period (hr)
hCRY2-WT-Tg #1
hCRY2-WT-Tg #2
hCRY2-A260T-Tg #1
hCRY2-A260T-Tg #2
non-Tg
mCry2 KO
F
Relative Bioluminescence
Time (hr)
CRY2-WT
CRY2-A260T
Period (hr)
CRY2-WT
CRY2-A260T

Figure 3

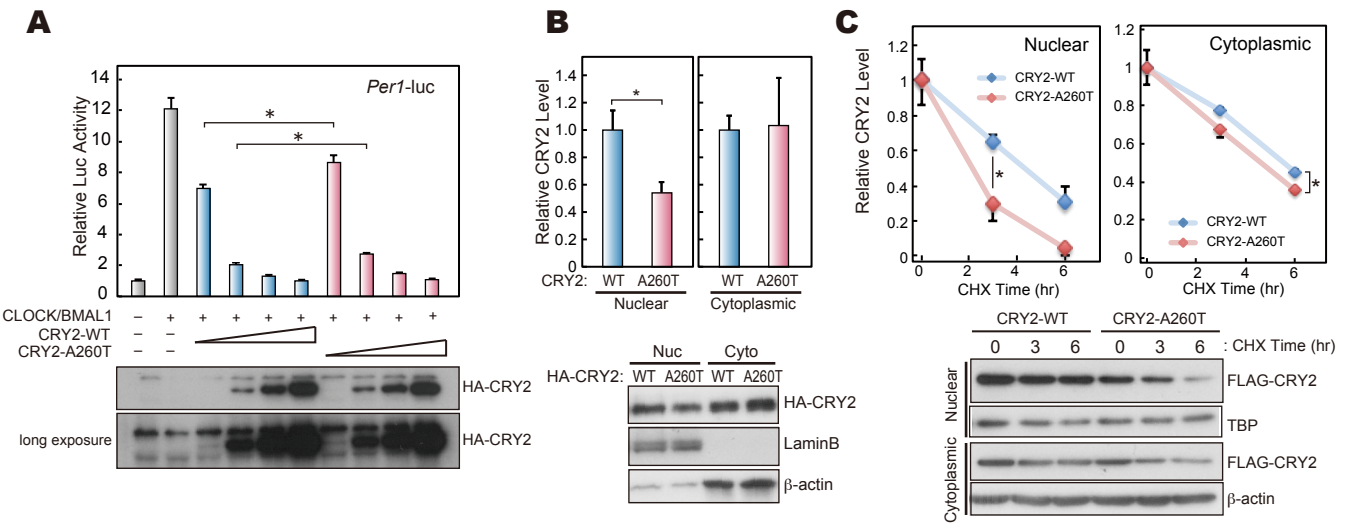
A
Per1-luc
Relative Luc Activity
CLOCK/BMAL1
CRY2-WT
CRY2-A260T
HA-CRY2
long exposure
HA-CRY2
B
Relative CRY2 Level
CRY2: WT A260T WT A260T
Nuclear
Cytoplasmic
Nuc Cyto
HA-CRY2: WT A260T WT A260T
HA-CRY2
LaminB
β-actin
C
Nuclear
Cytoplasmic
Relative CRY2 Level
CRY2-WT
CRY2-A260T
CHX Time (hr)
CRY2-WT CRY2-A260T
0 3 6 0 3 6 : CHX Time (hr)
Nuclear
Cytoplasmic
FLAG-CRY2
TBP
FLAG-CRY2
β-actin

Figure 4

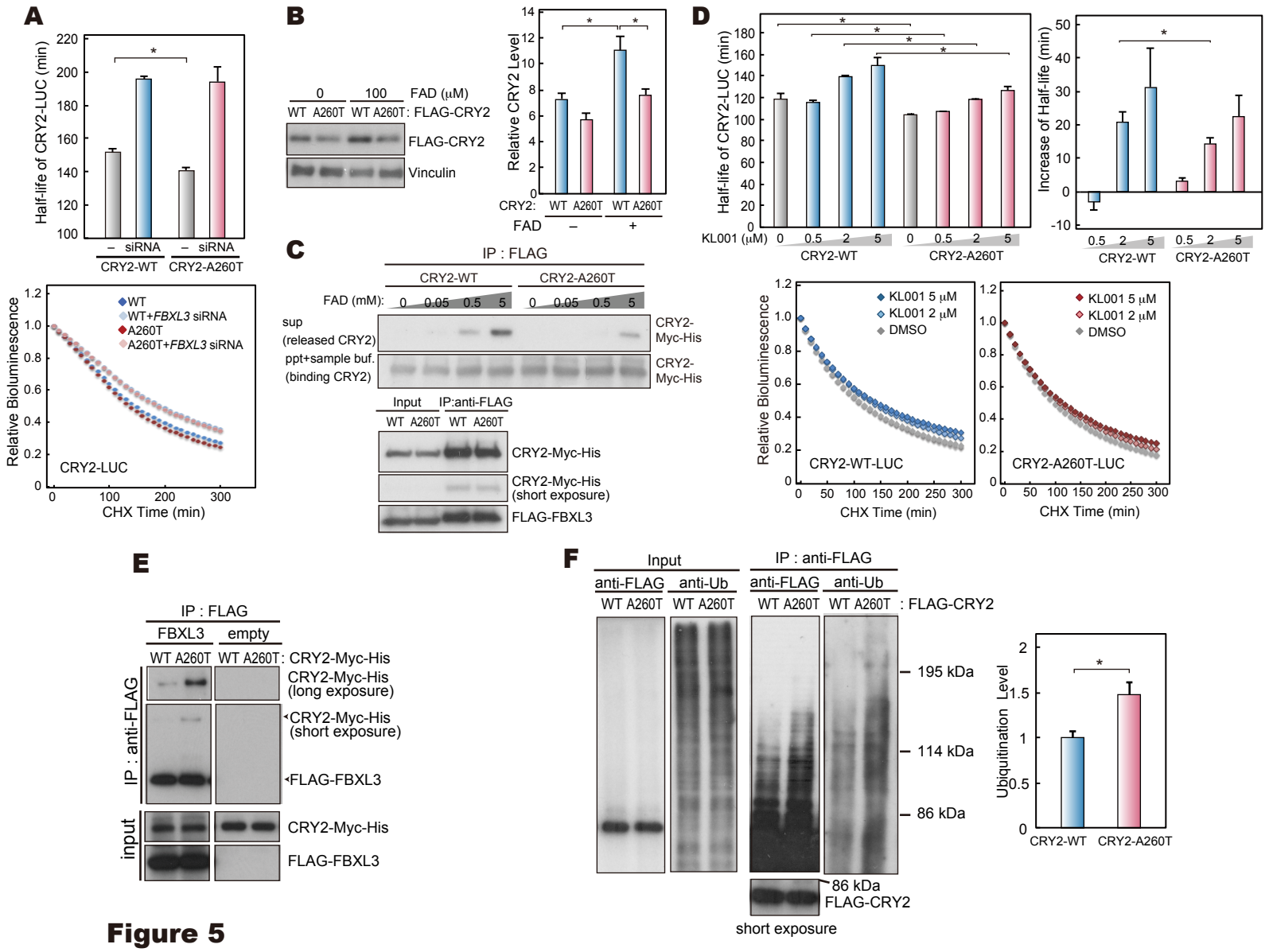
A
Half-life of CRY2-LUC (min)
– siRNA
– siRNA
CRY2-WT
CRY2-A260T
Relative Bioluminescence
WT
WT+FBXL3 siRNA
A260T
A260T+FBXL3 siRNA
CRY2-LUC
CHX Time (min)
B
0
100
FAD (μM)
WT A260T WT A260T: FLAG-CRY2
FLAG-CRY2
Vinculin
Relative CRY2 Level
CRY2: WT A260T WT A260T
FAD – +
C
IP : FLAG
CRY2-WT
CRY2-A260T
FAD (mM): 0 0.05 0.5 5 0 0.05 0.5 5
sup
(released CRY2)
ppt+sample buf.
(binding CRY2)
CRY2-Myc-His
Input
IP:anti-FLAG
WT A260T WT A260T
CRY2-Myc-His
CRY2-Myc-His
(short exposure)
FLAG-FBXL3
D
Half-life of CRY2-LUC (min)
KL001 (μM) 0 0.5 2 5 0 0.5 2 5
CRY2-WT
CRY2-A260T
Increase of Half-life (min)
0.5 2 5 0.5 2 5
CRY2-WT
CRY2-A260T
Relative Bioluminescence
KL001 5 μM
KL001 2 μM
DMSO
CRY2-WT-LUC
CRY2-A260T-LUC
CHX Time (min)
E
IP : FLAG
FBXL3
empty
WT A260T WT A260T: CRY2-Myc-His
IP : anti-FLAG
CRY2-Myc-His
(long exposure)
CRY2-Myc-His
(short exposure)
FLAG-FBXL3
input
CRY2-Myc-His
FLAG-FBXL3
F
Input
IP : anti-FLAG
anti-FLAG anti-Ub
anti-FLAG anti-Ub
WT A260T WT A260T WT A260T WT A260T : FLAG-CRY2
195 kDa
114 kDa
86 kDa
86 kDa
FLAG-CRY2
short exposure
Ubiquitination Level
CRY2-WT
CRY2-A260T

Figure 5

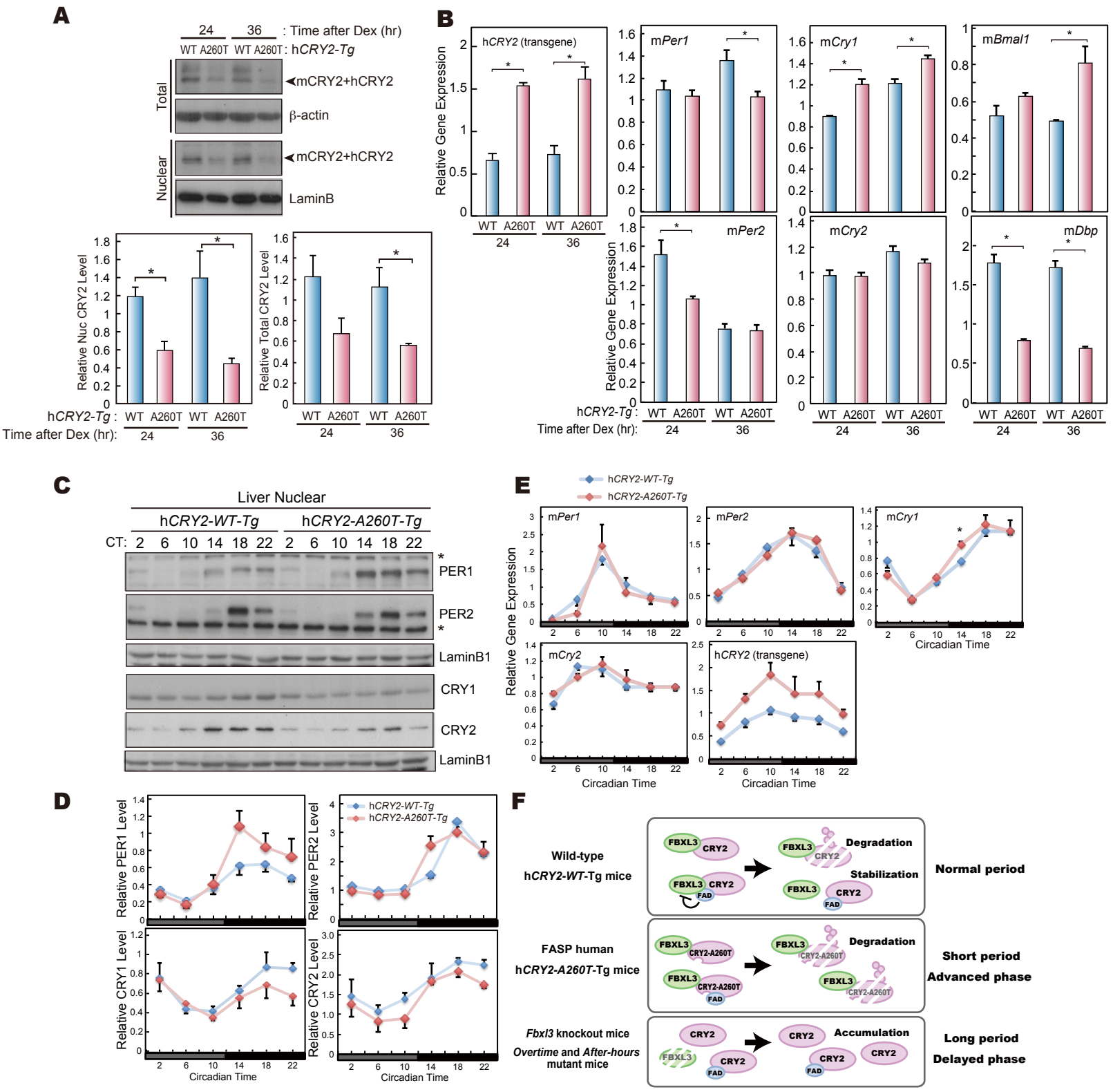
A
24
36
: Time after Dex (hr)
WT A260T WT A260T : hCRY2-Tg
Total
mCRY2+hCRY2
β-actin
Nuclear
mCRY2+hCRY2
LaminB
Relative Nuc CRY2 Level
Relative Total CRY2 Level
hCRY2-Tg : WT A260T WT A260T
Time after Dex (hr): 24 36
B
hCRY2 (transgene)
mPer1
mCry1
mBmal1
mPer2
mCry2
mDbp
Relative Gene Expression
C
Liver Nuclear
hCRY2-WT-Tg
hCRY2-A260T-Tg
CT: 2 6 10 14 18 22 2 6 10 14 18 22
PER1
PER2
LaminB1
CRY1
CRY2
LaminB1
D
Relative PER1 Level
Relative PER2 Level
Relative CRY1 Level
Relative CRY2 Level
hCRY2-WT-Tg
hCRY2-A260T-Tg
Circadian Time
E
hCRY2-WT-Tg
hCRY2-A260T-Tg
mPer1
mPer2
mCry1
mCry2
hCRY2 (transgene)
Relative Gene Expression
Circadian Time
F
Wild-type
hCRY2-WT-Tg mice
FBXL3
CRY2
FAD
Degradation
Stabilization
Normal period
FASP human
hCRY2-A260T-Tg mice
CRY2-A260T
Degradation
Short period
Advanced phase
Fbxl3 knockout mice
Overtime and After-hours
mutant mice
Accumulation
Long period
Delayed phase

Figure 6

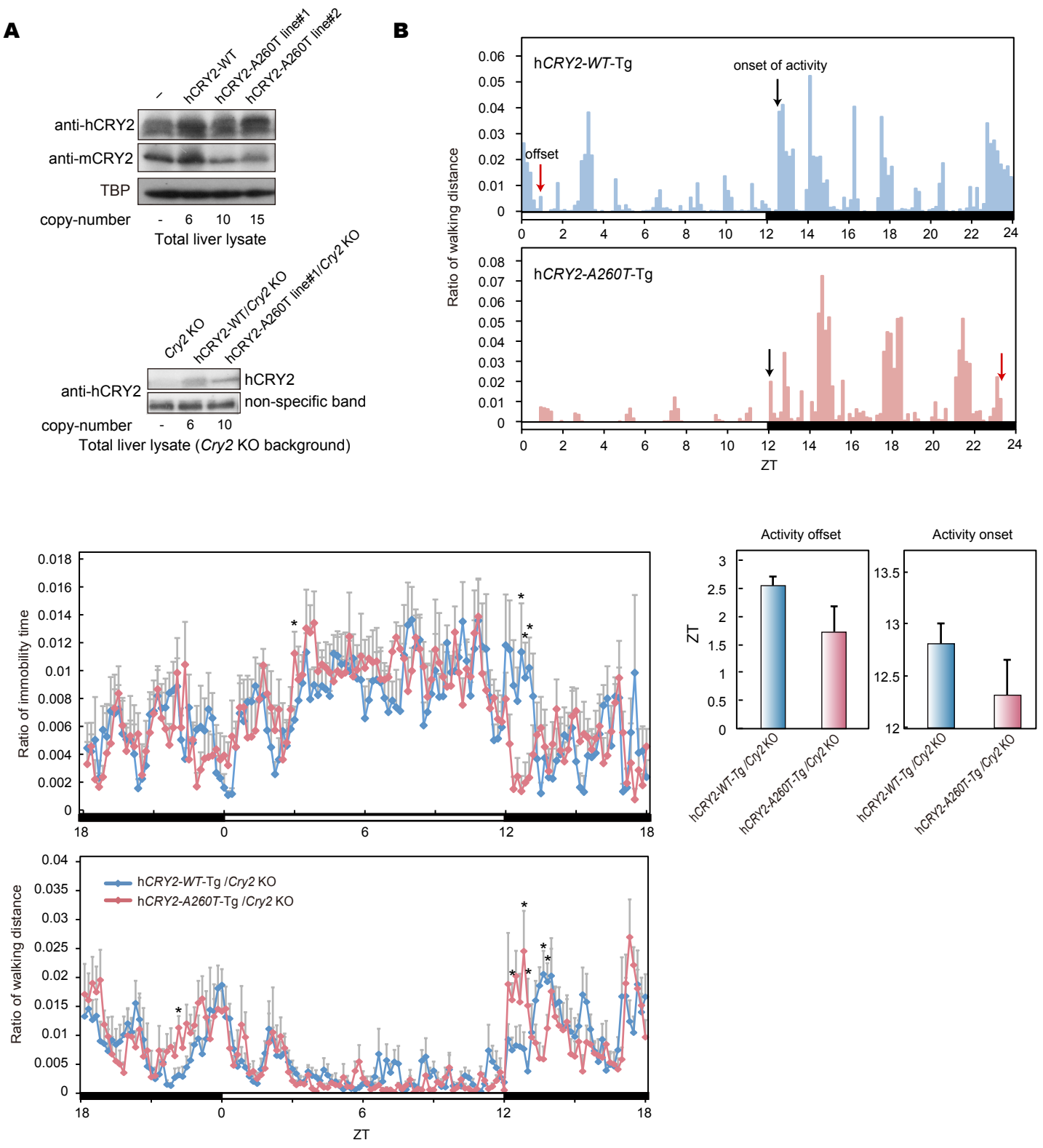

Figure 2-Supplement 1

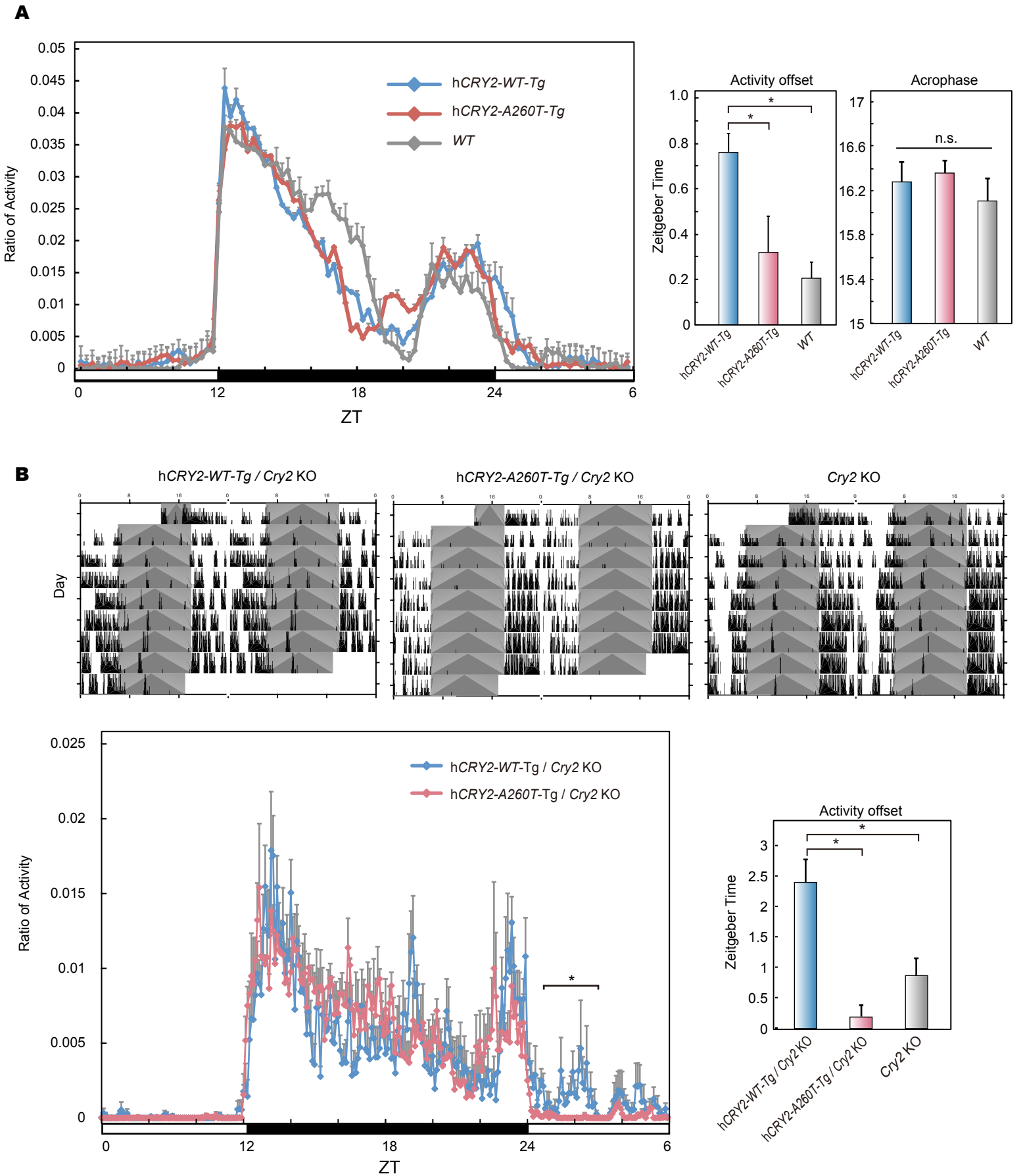

Figure 2-Supplement 2

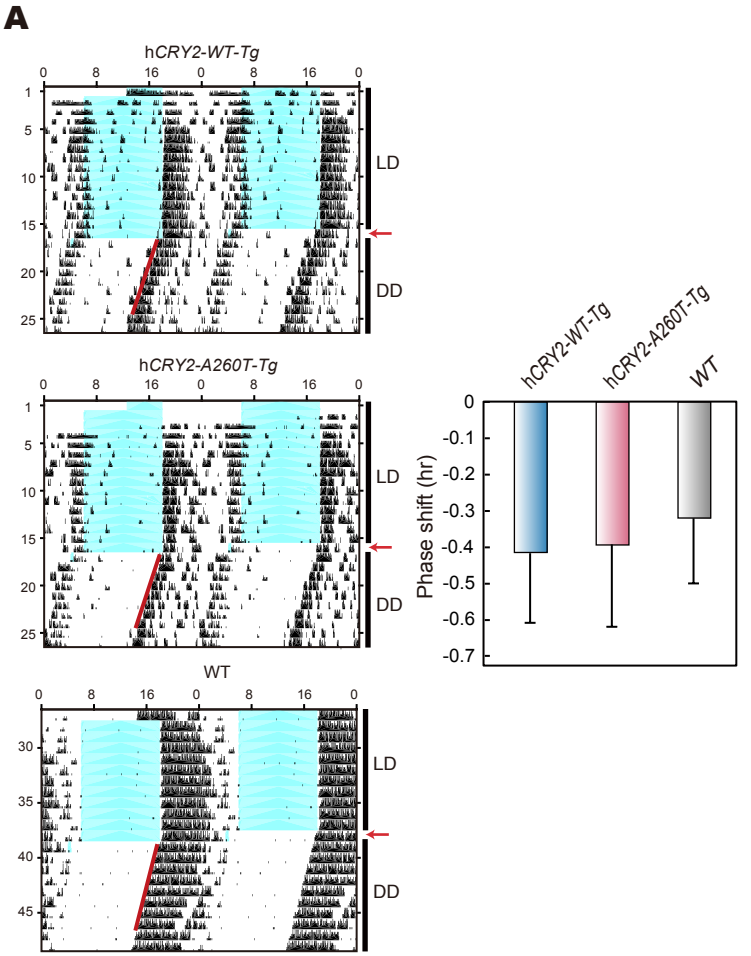

Figure 2 - supplement 3

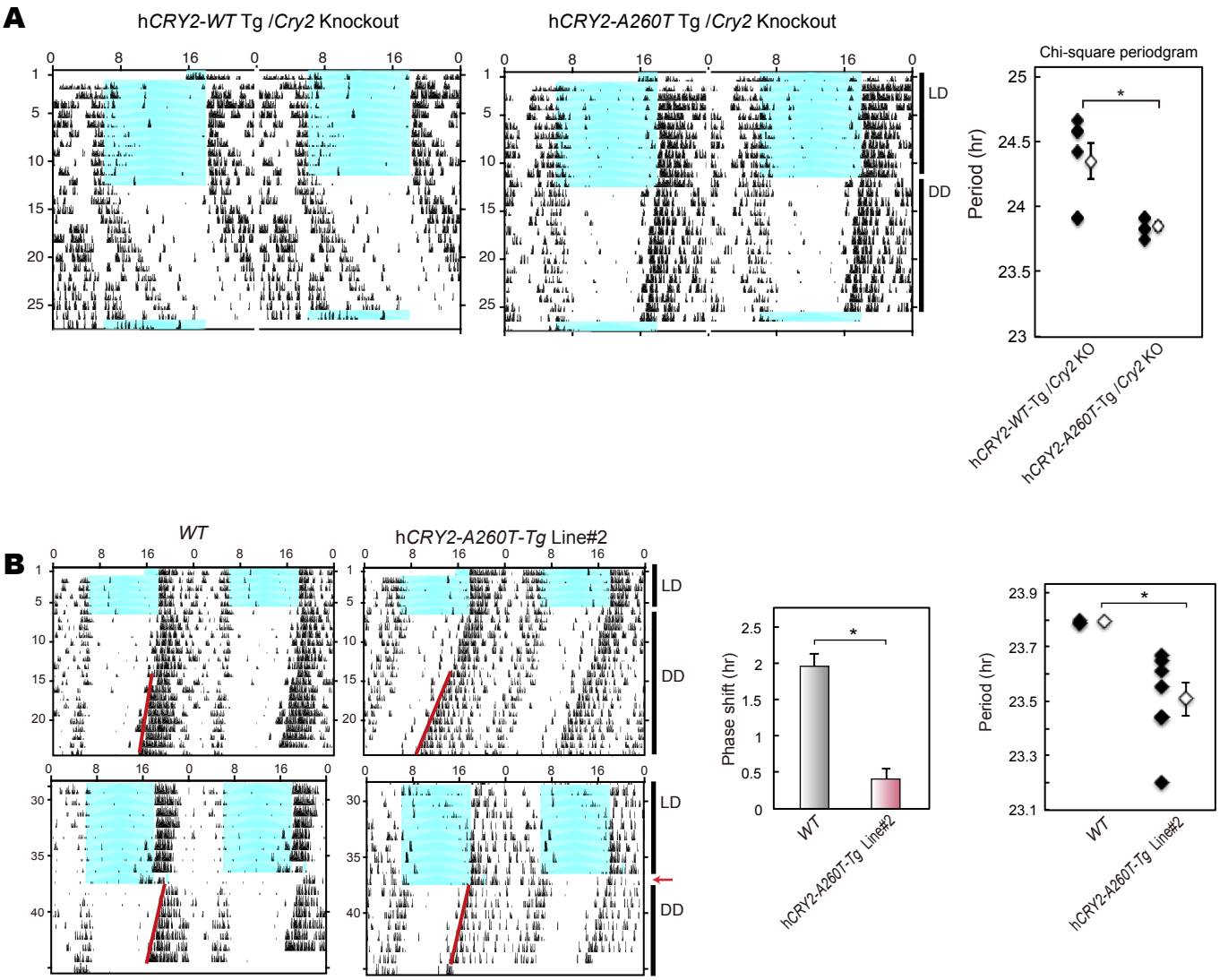

Figure 2 - supplement 4

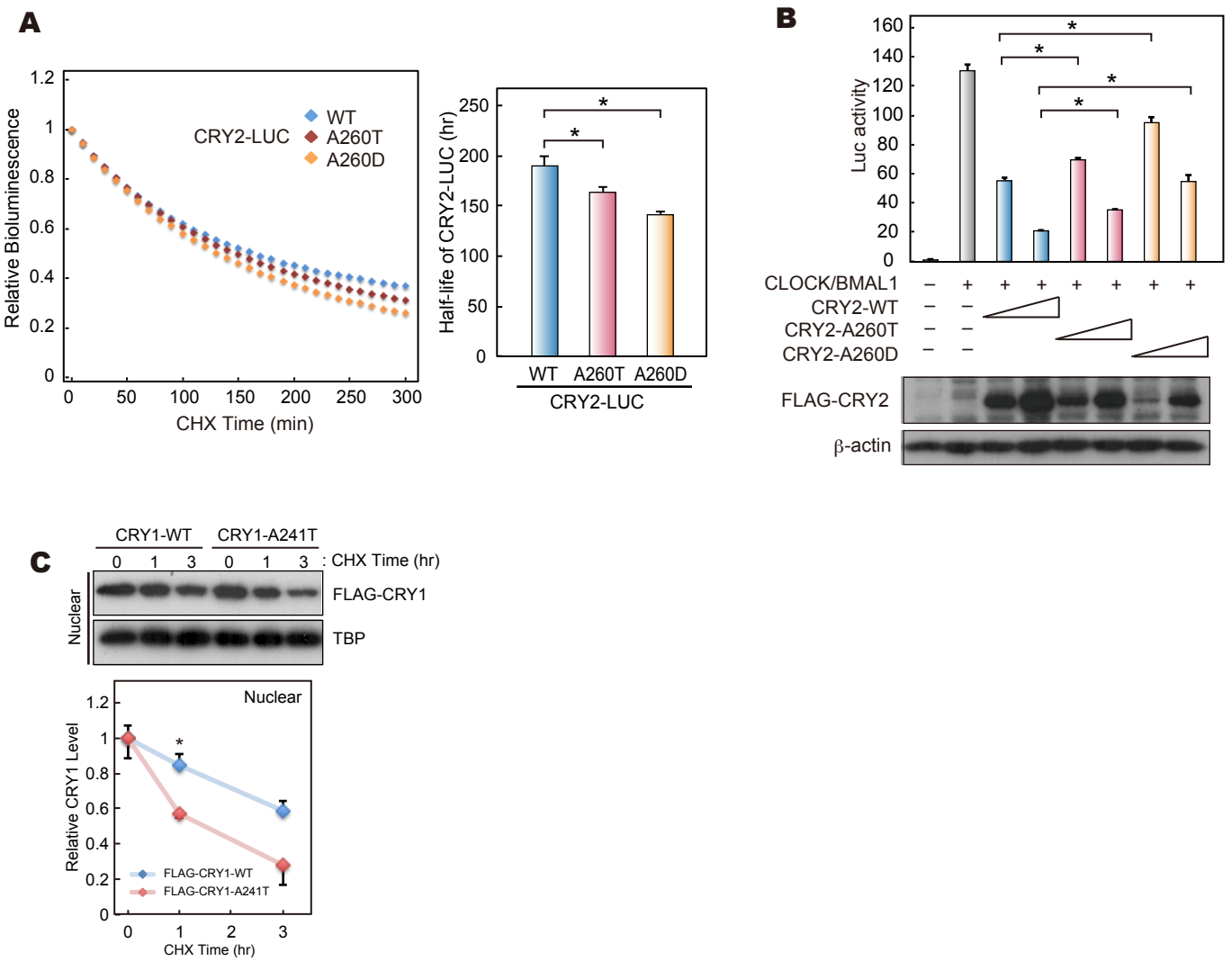

Figure 4 - supplement 1

A

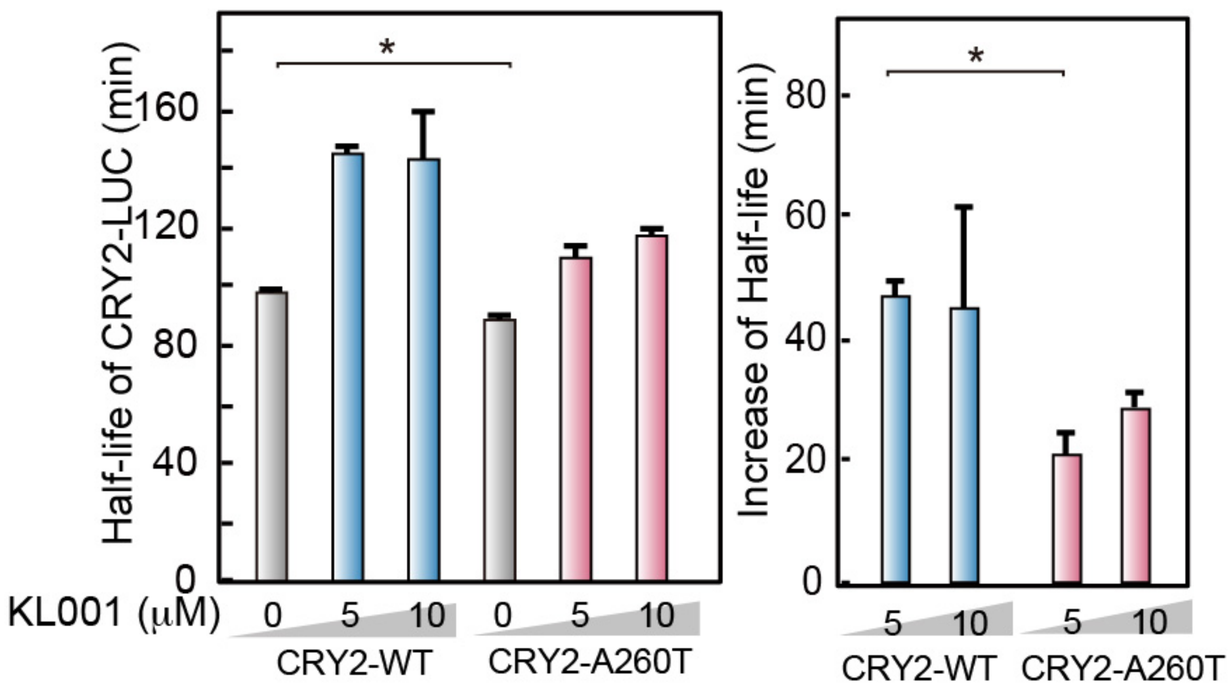

B

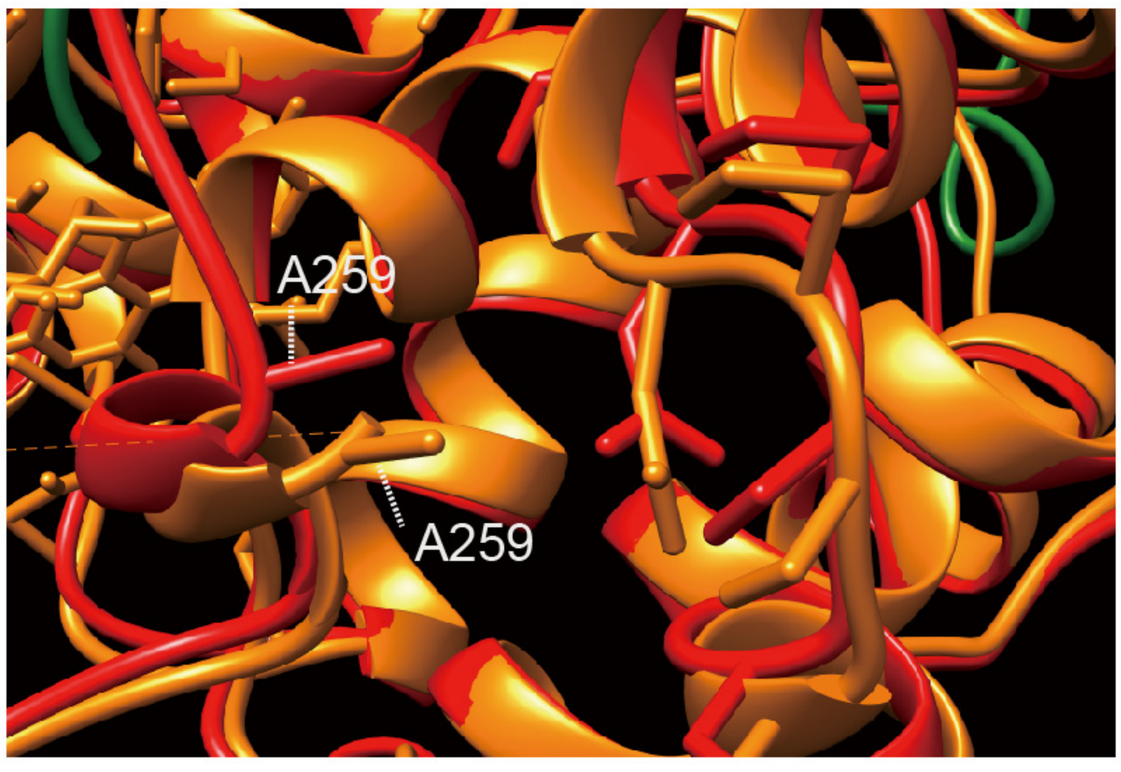

c

CRY2-WT

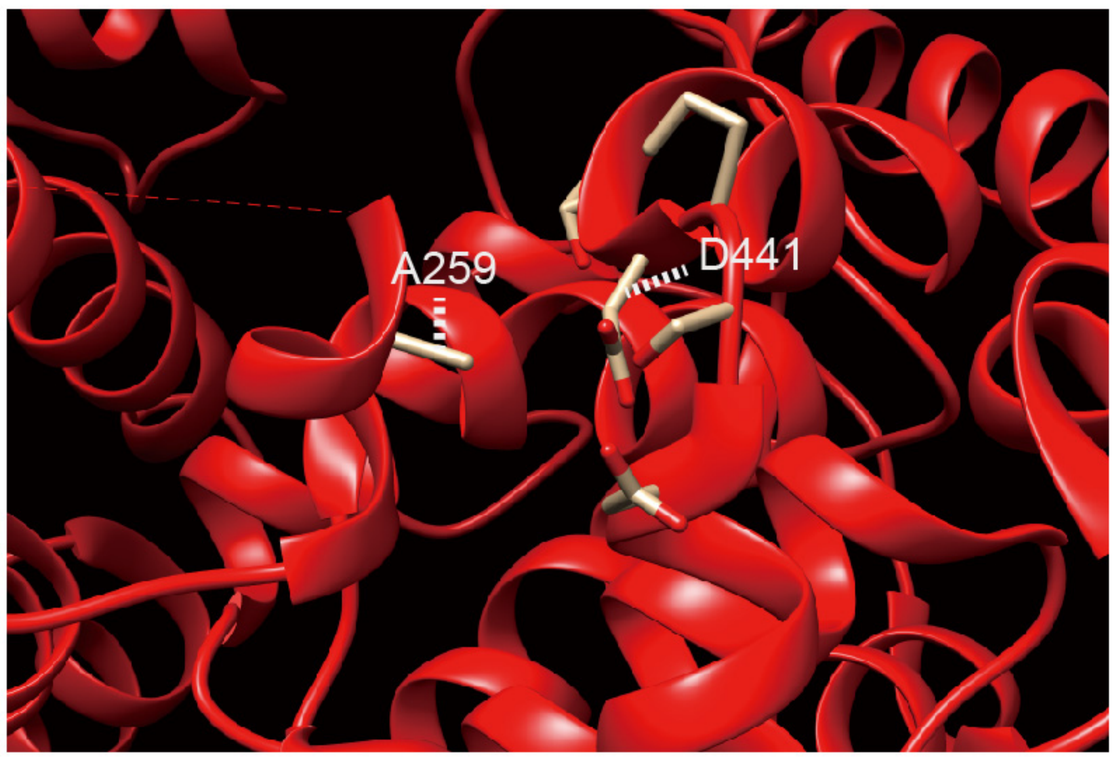

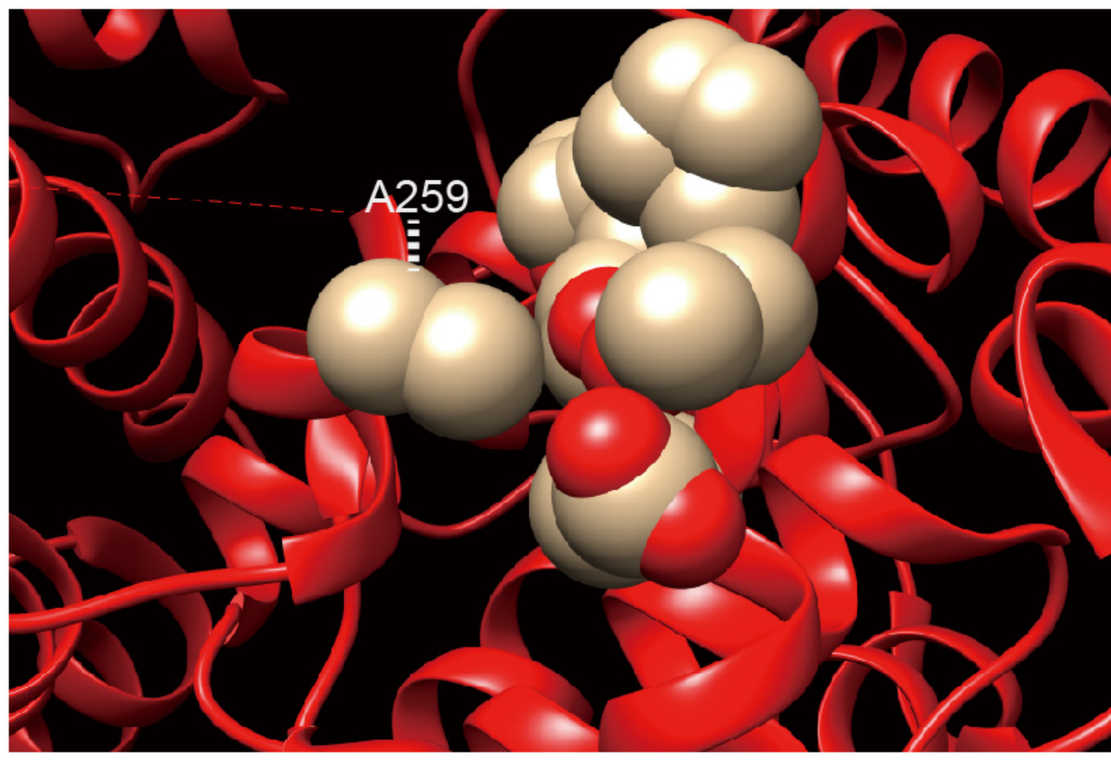

CRY2-A260T

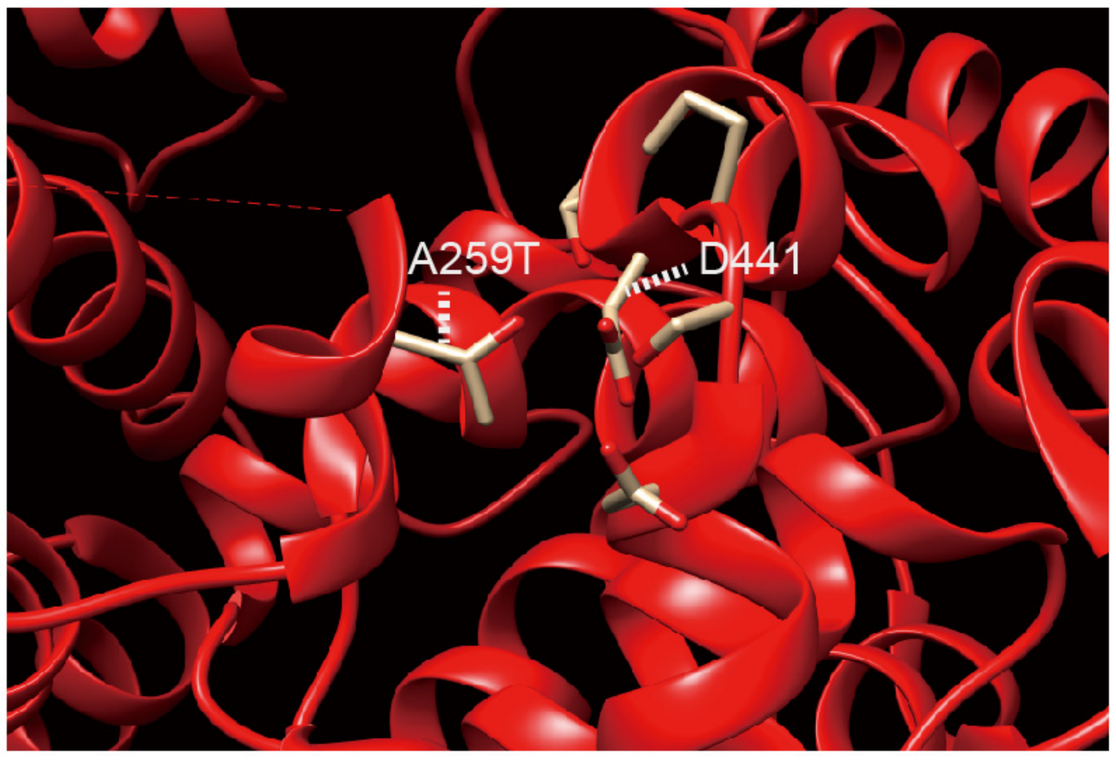

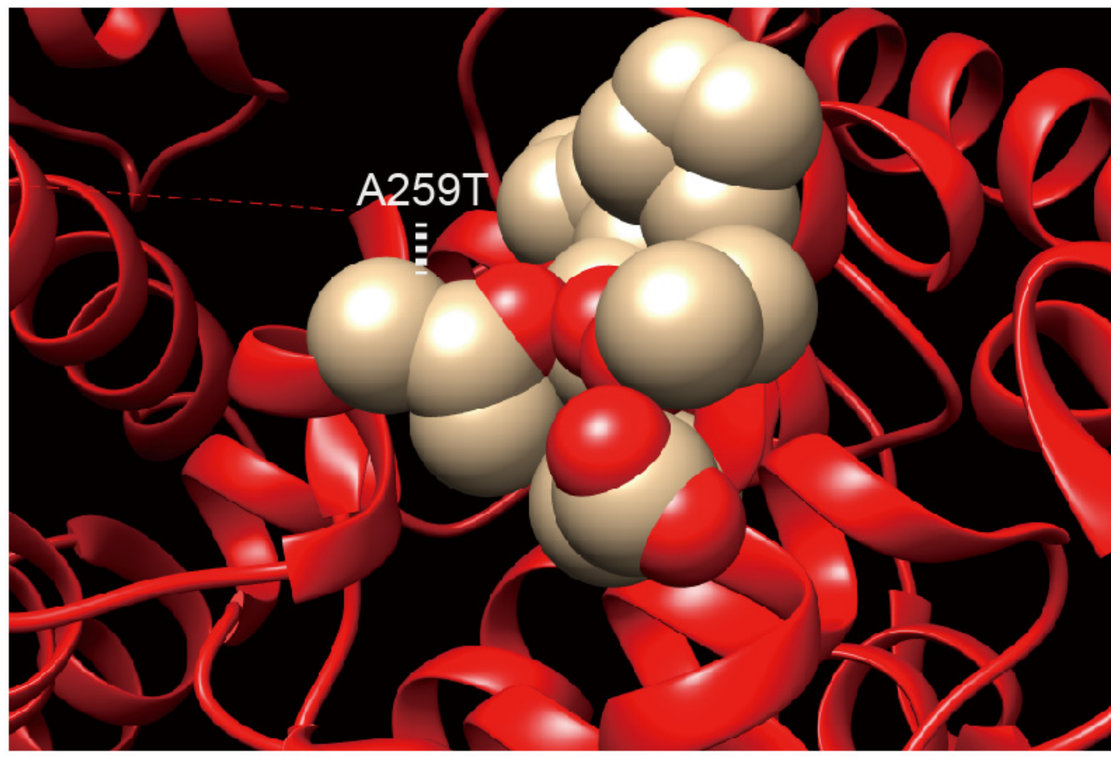

Figure 5 - supplement 1

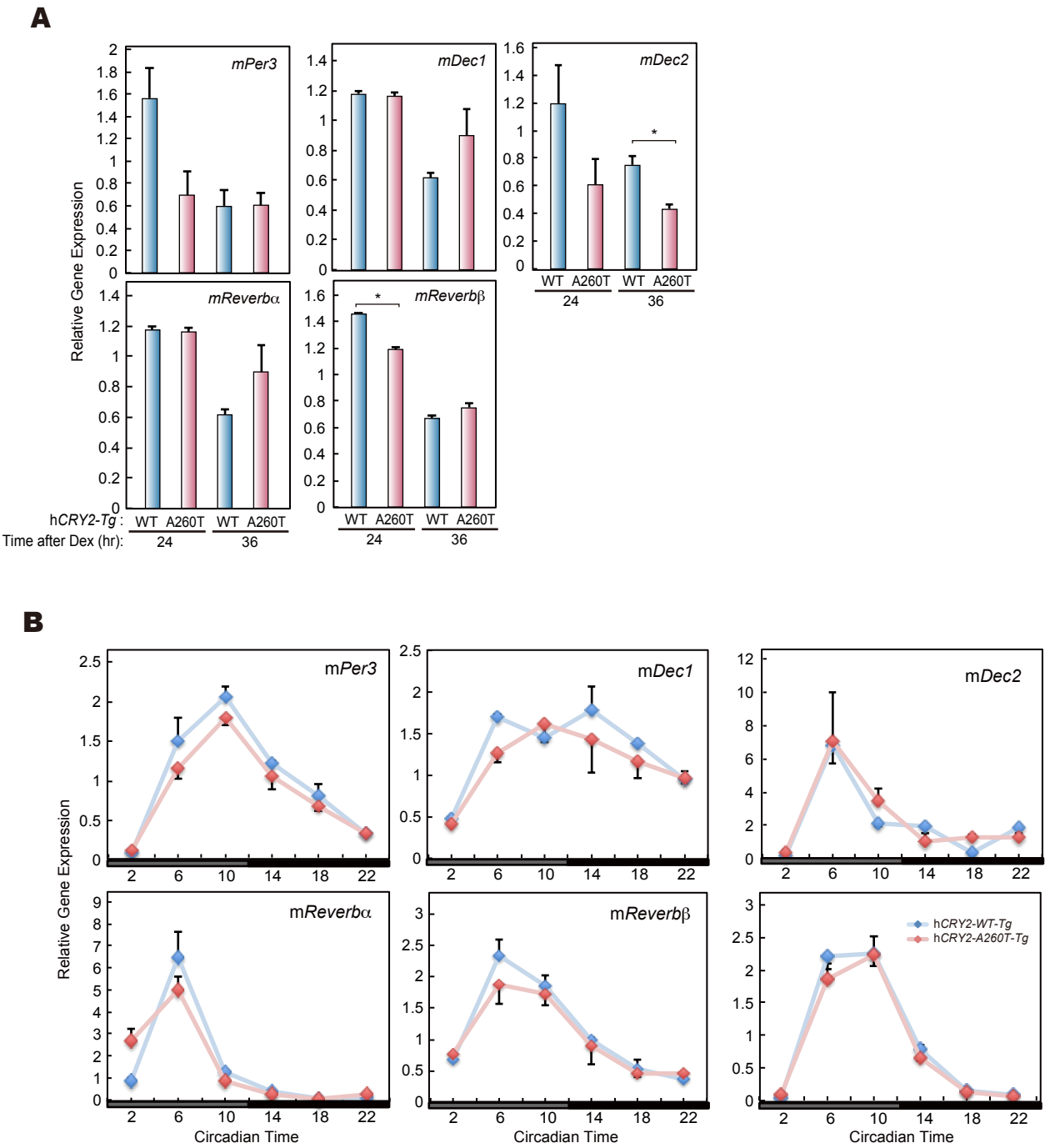

Figure 6 - supplement 1